DNA-encapsulated silver clusters on DNA-nanotube structures

Donny de Bruin

July 9th, 2013

Universiteit Leiden

Bachelor thesis based on research performed under supervision of:

Msc. N. Markešević
Dr. S.S.R. Oemrawsingh
Prof. Dr. D. Bouwmeester

As part of the Quantum Optics & Quantum Information research group at Leiden University.

Contents

Introduction

Single stranded DNA, or ssDNA, can be used to stabilize silver clusters of only a few atoms in size [1]. Studying these clusters is of substantial interest because their size places them in between the relatively well-understood molecular and nanoparticle regimes. As a result, whether their optical properties are the result of molecular or plasmonic behavior is a question of significant interest. In addition, the properties of these Ag:DNA's, and their optical activity, can be tuned through modifications to the DNA-encapsulation [2]. Visibly fluorescent Ag:DNA's are of particularly large interest as a result of their potentially high quantum yield, photostability and the tunability of the emission wavelength through modification of the hosting DNA-strand.

Utilizing the binding specificity of Watson-Crick basepairing, DNA can be programmed to produce nanostructures through self-assembly processes [3]. Combining fluorescent Ag:DNA's with larger DNA nanostructures allows placement of fluorescent emitters on a nanometer scale [4]. Placing these fluorophores with such precision will make it possible to observe possible optical interactions in the near-field, including FRET, or quenching and enhancement behavior. ssDNA's can stabilize multiple types of fluorescent silver clusters, with varying emission spectra within a 30-40nm wavelength range [5]. Because of this, frequency pulling in the emission from the spectrally slightly different emitters is another interesting possibility.

To enable us to use DNA-nanostructures to house Ag:DNA's reliably and accurately, the placement of the emitters on DNA-structures and the interactions between the Ag:DNA and its host have to be properly understood. Additionally, observation of any interactions between the Ag:DNA's and more complicated structures can give us an insight in the behavior of the silver cluster and its encapsulation.

The results as presented in this thesis will be aimed at developing our understanding of DNA-encapsulated silver clusters on DNA-nanostructures, and will be based upon a comparison between individual fluorescent Ag:DNA's, and their equivalents placed in close proximity on two types of DNA-nanotube.

Part I

Theory and Methods

Chapter 1

Theory

1.1 DNA-encapsulated silver clusters

ssDNA can be used to stabilize silver in solution to form clusters which are only a few atoms in size [1], utilizing the following process: Silver ions can be introduced to the DNA-strands in solution, which will be attracted to the negatively charged DNA-backbone (Figure 1.1). After the silver ions have been allowed to bind to the DNA-bases, a reducing agent can be added, changing some of the ions within the silver clusters to their uncharged state. In this process, the silver will be stabilized into silver clusters of sizes and configurations depending on the properties of the encapsulation. Cytosine- and guanine-bases have been shown to have the greatest involvement in silver cluster formation [2]. Depending on the sequence of the DNA-host, the silver clusters can form fluorescent species that are active in the visible range.

The properties of the environment have been known to have a large effect on the optical properties of these DNA-encapsulated silver clusters. Changes in pH and in the chemical composition of the solution can have an large effect on silver cluster formation, and on the fluorescence of these emitters. Additionally, changes in temperature are expected to have a significant effect on the properties of the silver cluster and its encapsulation.

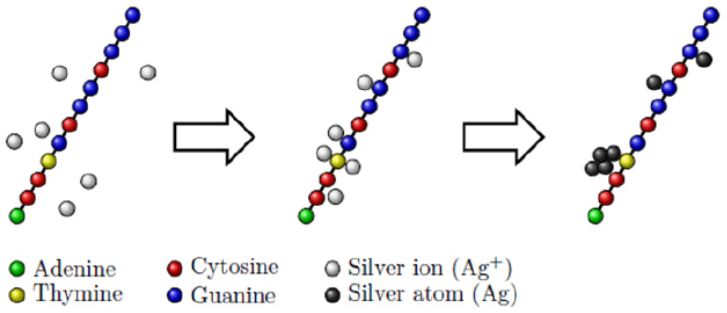

Figure 1.1: Cartoon of the formation of a silver cluster on a DNA-strand. Individual silver ions are attracted to the negatively charged DNA-backbone. A reducing agent is added to change part of the silver ions into their uncharged state. In the process, few-atom silver clusters will form.

In order to pre-determine the position of the silver cluster on the ssDNA, base-pairing can form a double-stranded part to leave a single-stranded loop to catch the silver ions (Figure 1.2). The size and sequence of the loop will determine the final properties of the encapsulation, and which sizes and configurations of silver clusters can be present within [2, 6]. In addition, the double-stranded part, known as the stem, will determine the rigidity of the structure, meaning the breaking of the

base-pairs in this stem will determine the way the silver cluster behaves when the temperature is raised.

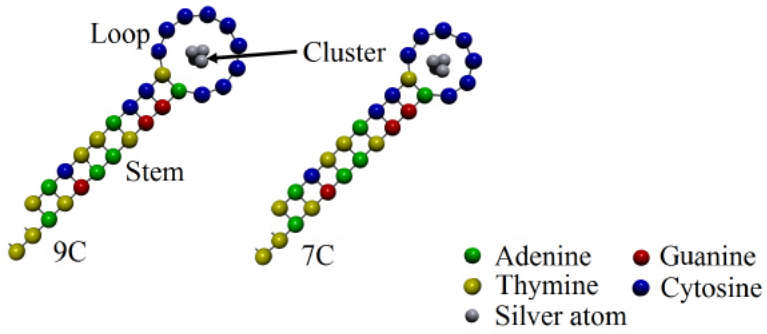

Figure 1.2: *Cartoon of the single-stranded hairpin structure. The loop allows formation of different sizes and shapes of silver cluster, generally of smaller size than the actual hairpin, which is 9 or 7 bases, or between 2nm and 3nm, in circumference.*

A specific ssDNA sequence can allow the formation of silver clusters differing in structure and size, with different optical properties as a result. It has been shown that the relative emission gathered from these different emitter types show a degree of coupling in their behavior over time [6].

1.2 DNA-nanotubes

The pairing nature of single stranded DNA can be used to design and build structures on a nanometer-scale using self-assembly methods [3, 7]. For the experiments in this thesis, simple DNA-structures were built to house silver clusters using a similar self-assembly process. Two different types of DNA-structure will be discussed, DX-nanotubes, based on a multi-stranded tile structure, and 6HX-nanotubes constructed out of single-stranded tiles.

1.2.1 DX-nanotubes

The DX-nanotubes are based on a multi-stranded tile system (Figure 1.3). Five DNA-strands form identical tiles through base-pairing, which stack together into a ribbon through 20 un-paired bases called 'sticky ends'. An inherent curve is present on the tiles due to the helicity of the DNA-strands, causing the ribbon to curve into a tube. Because there are 20 base-pairs involved in the bonds between the tiles, and this is much fewer than the 74 base-pairs that form the individual tiles, the tiles have a higher melting temperature than the tube structure they form in order to ensure the annealing occurs properly.

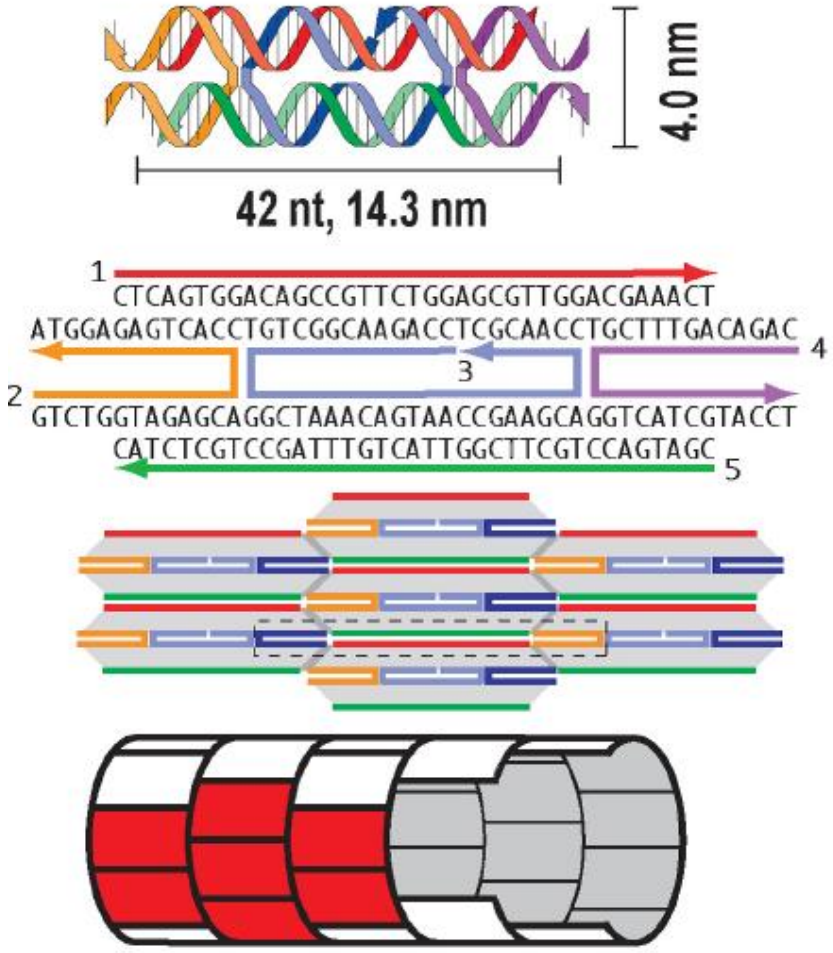

Figure 1.3: *Cartoon of the DX-nanotube structure. The 5 individual strands form tiles with 'sticky ends' (strands 2 and 4), allowing a stacking process to form a larger ribbon-like structure. Inherent helicity of the strands causes the ribbon to form into a tube [4].*

By modifying the individual tiles, hairpins can be added to the structure to allow formation of fluorescent silver clusters attached to the tube (Figure 1.4). A longer stem, from here on referred to as the 'jstem', is used, to allow the silver clusters to form properly without interference from the tube. One strand of the stem is lengthened by addition of two Thymine-bases to align the stems with the tube. As a result, the hairpins are expected to be close to the tube structure.

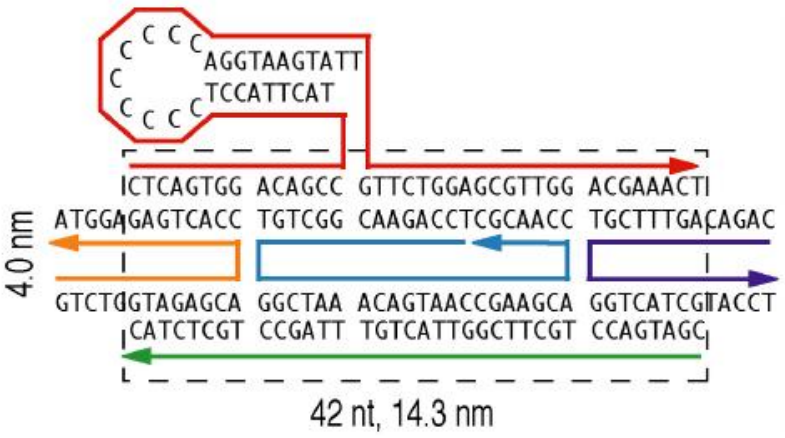

Figure 1.4: *Modified version of the tile-structure in Figure 1.2. In this case, a 9C-hairpin is added to strand 1 to allow emitters to form on the tube [4].*

1.2.2 6HX-nanotubes

The 6HX-nanotubes reported on in this thesis are based on a single stranded tile structure (Figure 1.5). Unlike the DX-tubes, each tile on the circumference consists of a single DNA-strand, meaning the tiles along resulting circumference will not be identical. With regard to our experiments, these tubes will have an advantage over the DX-nanotube constructions because modifications to a single strand will take on a well-defined spot on the circumference of the tube, and relative to other modified strands.

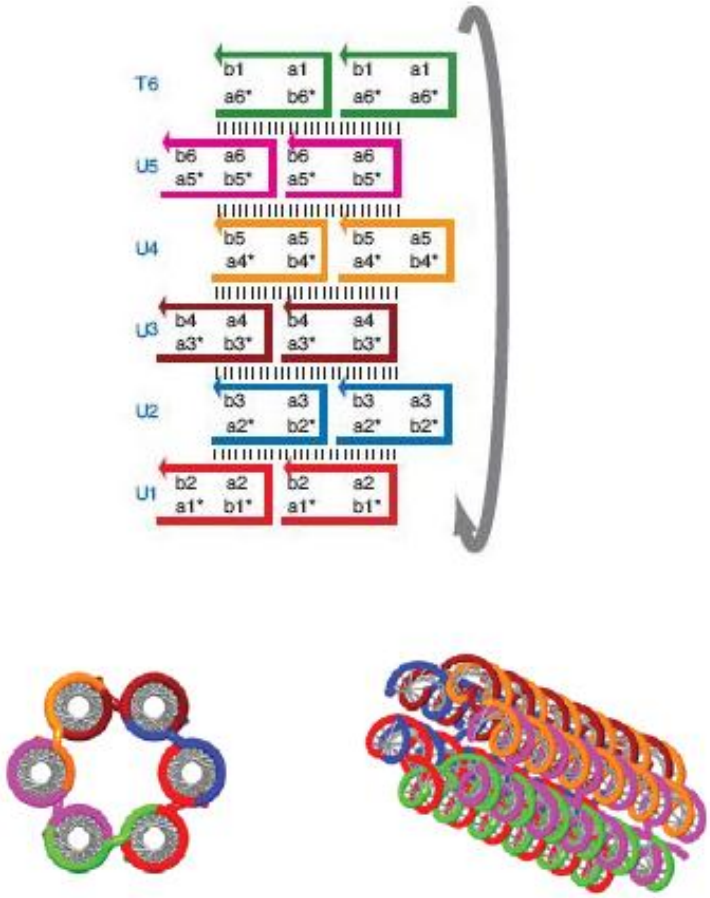

Figure 1.5: *Cartoon of the 6HX-nanotube tile structure (top), and the predicted shape of the 6HX-nanotubes (bottom) [8]. Six strands form base-pairs with two other strands each, allowing a closed structure to form.*

The self-assembly process should form tubes of a 6nm diameter, and an average length of 6μm. Whilst multiples of the 6 individual strands can also theoretically form tube-structures, the process has been shown to produce 6nm tubes with a high monodispersity [8].

Modifications have been made to the 5'-end of the U3-strand, and to the 3'-end of the U5-strand, in order to allow silver clusters to be placed onto the tube structure. A dye-molecule in the form of Cy3 has been added to the 5'-end of U1 in order to ensure visibility under a fluorescence microscope. The reason for choosing Cy3 for this purpose is its potential in acting as a donor in FRET-activity involving Ag:DNA's, allowing further insight into the placement of the emitters on these nanotubes.

1.3 Förster Resonance Energy Transfer

Förster Resonance Energy Transfer, or FRET, is a process whereby two nearby dipoles can induce an energy transfer when one of the dipoles is excited. The process involves electrostatic interactions between the two charge distributions of the two molecules, causing the energy 'donor' to decay from the excited state into its ground state, while the 'acceptor' is excited.

The presence of FRET is based upon a fairly small distance between the two relevant dipoles, with its efficiency defined as [9]:

$$E = \frac{1}{1+(r/R_0)}$$

Whereby R_0 is known as the Förster radius and is defined as:

$$R_0^6 = ck^2n^{-4}Q_D J(\lambda)$$

c being a constant ($8.786 \cdot 10^{-11}$), k^2 being an orientational factor which can be estimated at $2/3$ for isotropic distributions, n the refractive index of the medium, and Q_D the quantum yield of the donor.

$J(\lambda)$ is the overlap integral between the emission spectrum of the donor and the absorption spectrum of the acceptor, and is defined as:

$$J(\lambda) = \int_0^\infty F_D \epsilon_A \lambda^4 d\lambda$$

Whereby F_D is the normalized emission spectrum of the donor, and ε_A is the molar absorptivity of the acceptor.

This overlap integral has a relatively large influence on the size of the Förster radius, meaning the distance over which FRET will be observed is highly dependent on the spectral overlap between the emission of the donor and the absorption of the acceptor. Generally, a Förster radius between 5-8nm is to be expected for well-matched pairs [9].

1.4 Injection Locking

Because the Ag:DNA's that can be formed based on a given DNA-strand sequence vary spectrally within a certain wavelength range [5], observing a process known as injection locking may be possible between spectrally different emitters on DNA-nanotubes.

When a harmonic oscillator is coupled to another which operates at a nearby frequency, the second oscillator can change the frequency of the first to its own, in a process known as injection locking. Depending on the level of coupling, it can manifest in smaller form, known as injection- or frequency pulling, whereby the operating frequency of the first oscillator is merely disturbed and brought closer to the frequency of the second. Originally, this phenomenon was first properly understood for LC-circuit based resonators [10], and later generalized for other oscillating systems [11]. It is now frequently used in lasers to 'purify' the output wavelength further through injection of another laser at the desired frequency [12].

Adler's original equation for harmonic oscillators [10] (to be precise, for LC-circuits) gives an insight into injection locking behavior:

$$\frac{d\triangle\phi(t)}{dt} = \triangle f_0 - \frac{I_i}{I_R}\frac{f_0}{2Q} sin(\triangle\phi(t))$$

Δf_0 is the frequency difference between the two oscillators, $\Delta\phi$(t) the phase difference. Q is the quality factor of the system, and I_i and I_R are the injected current and the current of the original resonator, respectively. When the two oscillators are fully locked, the phase difference will be a constant, and the maximum difference between the two oscillators, or the 'locking range', will be strongly dependent on the relative amplitudes of the two oscillators.

Chapter 2

Methods

2.1 Sample preparation

2.1.1 Single emitters

The Ag:DNA's used in these experiments included two different types of hairpin-based emitters, 7C and 9C, named as such because of the amount of cytosine-bases present in their individual loops. An emitter based on an ssDNA without a pre-defined double-stranded part, called 'Rockstar', is also used. These emitters were chosen for our experiments because they have been shown to allow formation of visibly and intensely fluorescent silver clusters.

The 7C-/9C hairpins, with varying stems, were purchased from Integrated DNA Technology, Inc., and used without further purification (this is the case for all the oligonucleotides used in the experiments presented in this thesis). The synthesis of the silver clusters follows a procedure which is known to produce visibly fluorescent Ag:DNA's [2, 6]. Silver was introduced to the DNA-hairpins in the form of $AgNO_3$ in an NH_4OAc buffer, after which the mixture was left refrigerated ($\sim 4^oC$) for 30 minutes before the reduction was started by addition of $NaBH_4$. A 9:1 [Ag/DNA] ratio was used for the 7C-hairpins, and a 7:1 [Ag/DNA] ratio was used for the 9C-hairpin samples. The [$NaBH_4$/Ag] ratio was 1:5.4 for the 7C-hairpins, and 1:3.5 for the 9C equivalents (exact concentrations used can be found in Appendix B.). These ratios are the ones used in previous experiments involving these Ag:DNA's, and yield emitters with good enough emission peaks around a 640nm emission wavelength for them to be used in these experiments.

For synthesis of the emitters on 'Rockstar'-strands, a 9.6:1 [Ag/DNA] ratio was used, again introduced in the form of $AgNO_3$, in the same NH_4OAc buffer. The reduction was initiated by addition of $NaBH_4$ in a 1:2 [$NaBH_4$/Ag] ratio. In the process of arriving at this procedure, the time between addition of silver and addition of the reducing agent was increased from 30 to 40-45 minutes, and the [Ag/DNA] ratio reduced from a starting value of 12.5:1, because there seemed to be a rather large excess of silver left in the solution after 30 minutes (visible in the form of an orange color). After this first round of optimization the emission from the emitters was good enough for the experiments discussed in this thesis, so the recipe and procedure have not been optimized further.

2.1.2 DX-nanotubes

The production of the DX-nanotubes is based on the procedure as published out by O'Neill et al. in 2012 [4]. The five strands comprising the tiles were mixed stoichiometrically in an NH_4OAc and MgOAc buffer in a thin-walled 200µL PCR tube, after which the mixture was placed in a hot water bath of around 90^oC. The water was allowed to cool down to room temperature slowly over a period between 2 and 4 days, during which the annealing process fully completes. In order to facilitate the addition of a silver cluster, the SE1-strand can be modified through addition of a 7C- or 9C-hairpin without compromising the tube structure. The SE3-strand can be modified

through addition of a fluorescein derivative, FAM, in order to make the bare tubes visible under a fluorescence microscope.

Silver clusters were synthesized on the DX-nanotubes as necessary using the same process as used by O'Neill et al. [4]. In most aspects the process is the same as the one used for forming individual 7C- or 9C-hairpin emitters, though a lower [Ag/DNA] ratio and a higher [$NaBH_4$/DNA] ratio was used for the synthesis of emitters on the tubes (exact concentrations used can be found in Appendix B.). These recipes have been seen to produce the best results. The lower silver concentration and higher concentration of the reducing agent should allow less interactions between the silver and the DNA-nanotube structure. The fact that less silver is used means that the chemical yield of the emitters forming on the tube will probably be lower than is the case for the individual hairpin-equivalent.

2.1.3 6HX-nanotubes

6HX-nanotubes were produced using a procedure based on the work of Peng Yin et al. as published in 2008 [8]. The 6 individual oligonucleotides were mixed stoichiometrically to a final concentration of 3μM in an NH_4OAc and MgOAc buffer. The buffer as used by Peng Yin et al. has been replaced because Ag:DNA's generally show a weaker fluorescence (due to a lower chemical- and/or quantum yield) when synthesized in a Tris-based buffer [4]. In the process, the Mg-concentrations were matched in order to allow the tube-structure to form properly. The pH of the buffer used in these experiments was lower than the Tris-based one used in earlier work on these tubes (pH 6.6 vs pH 7.6), which did not disturb the annealing process appreciably. The annealing process took place under the same conditions as those created for the DX-nanotubes (placed in 90^oC water, allowed to cool over 2-4 days).

In order to allow silver clusters to be formed on the 6HX-nanotubes, modifications to both the 5'-end of the U3-strand and the 3'-end of the U5-strand have been tried. In order to make the tubes visible under a fluorescence microscope, Cy3 was added to the 5'-end of the U1-strand. Cy3 is a dye from the Cyanine family which has a main emission peak around 565nm, and a secondary peak around 605nm, allowing it to be used as a donor in FRET-experiments involving Ag:DNA's. The modifications to the strands were chosen as to be positioned close enough to the Cy3 on the tube structure to use this feature, with estimated distances between 4 and 5nm.

Notable, but small, difficulties in the annealing process arise in the form of the DNA-strands clumping together to form relatively large (millimeters in length) string-like structures. The probability of this happening seems to increase when the mixture is placed in a centrifuge (2000RPM+, longer than 10seconds), or when larger modifications have been made to one or more of the individual strands. Even avoiding these conditions and keeping contamination to a minimum, this problem seems to arise in 1 out of 7 or 8 batches.

2.1.4 Fluorimetry

To observe the optical properties of a large number of Ag:DNA's, fluorimetry was performed on samples of the emitters in solution. The process involves spectroscopy on the emission while varying the excitation wavelength, to gain an overall understanding of the emisson from the different emitters that can form based on an individual ssDNA-strand.

The measurements performed on the sample in a 100μL quartz cuvette, using a Varian Cary Eclipse fluorescence spectrophotometer. The temperature of the solution was controlled using a water-cooled Peltier element attached to the cuvette-holder, after which the emission intensity was allowed to stabilize before measurements were made. All temperature measurements are based on a calibrated sensor outside of the cuvette.

Emission intensity estimates were made by taking a spectrum around peak emission, and averaging between 10 and 20 data-points around this peak, depending on the signal-to-noise ratio in the individual series of measurements.

2.1.5 Fluorescence Microscopy

In order to confirm the annealing process, and observe the DNA-nanotubes with or without fluorescent silver clusters (made visible through attached dyes), microscopy on the DX- or 6HX-tubes was performed using a Zeiss Axiovert 40 CFL confocal fluorescence microscope, with a 100x oil immersion objective. The samples were prepared by adding 4.5mg/ml PVA to the tube-solution, after which 50μL of the sample was spin-cast onto a clean glass coverslip for 2 minutes at 2000RPM. This process leads to around 2 cm^2 of PVA with embedded nanotubes, with a thickness in the micrometer range. The images as presented in this thesis are the result of averaging 100-200 frames of image data from an attached camera, in order to increase the signal-to-noise ratio. This averaging process was not necessary for the tubes to be observed in this setup.

2.1.6 Single Molecule Spectroscopy

A Single Molecule Spectroscopy setup (Figure 2.1) was used to perform spectroscopy on the emission from individual emitters, or on the emission from emitters on DNA-nanotubes. A dye-laser utilizing Rhodamine 590 tetrafluoroborate as dye is pumped by a 5 Watt 532nm laser. As a result, between 200 and 400 mW of usable laser power is produced with a wavelength tunable from 575 to 595nm. A noise-eater and a set of ND-filters is used to reduce the laser power to 5 mW while drastically reducing fluctuations in the intensity of the laser light. Imaging is done through addition of a wide-field lens into the excitation path. The laser power is reduced to 0.5 mW by use of ND-filterwheels when taking spectra or time-traces of the intensity of the emission.

20μL of the sample containing 4.5mg/ml PVA is spin-cast for 2 minutes at 4000RPM onto a fused silica substrate. The substrate is mounted in the focus of an objective and inserted into a cryostat, in which the objective can be moved along one axis. The cryostat is used to reduce the temperature of the sample to ∼220K using liquid nitrogen. The emission can be guided into a CCD-camera for imaging, or into an optical fibre, which can be fed into a spectrometer for spectral measurements, or into an APD for photon-counting.

When analyzing spectra taken using this setup, a Gaussian is used in data fits because these have been shown to be a reasonable approximation to the emission spectra obtained from Ag:DNA's [5].

All measurements performed using this setup at room temperature were done with the sample in air, with the blinking-activity of the emitters expected to be high as a result. Measurements at ∼220K were done in gaseous helium to prevent condensation of water vapour on the cryostat windows.

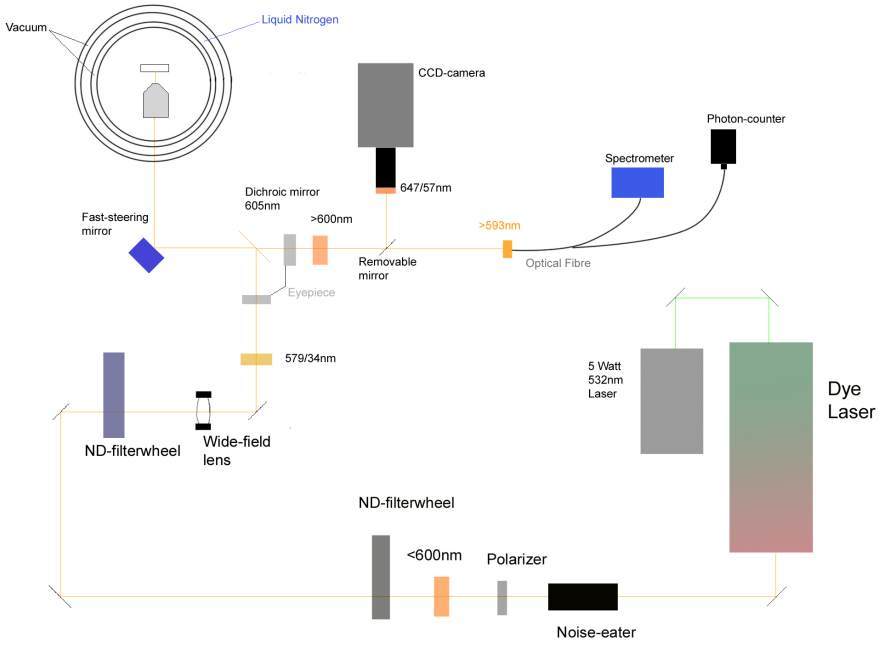

Figure 2.1: *Single Molecule Spectroscopy setup as used for emission wavelength spectroscopy and intensity time-traces. The laser is fed into a confocal setup consisting of a 579/34nm bandpass excitation filter, a dichroic mirror with a 605nm cutoff, and a 600nm longpass emission filter. A widefield-lens can be moved in and out of the beam in order to illuminate a larger part of the sample for imaging. The emission can be fed into CCD-camera, covered by a 647/57nm bandpass filter, for imaging. Alternatively, it can be lead through a 593nm longpass filter, into a spectrometer, for spectroscopy, or into a photon counter for intensity time-traces.*

Part II

Results

Chapter 3

Silver clusters on DX-nanotubes

3.1 7C-/9C-hairpin emitters

3.1.1 Spectral properties

Emission spectra of 7C- and 9C-hairpin based individual emitters were taken using the Single Molecule Spectroscopy Setup as described in Section 2.3.

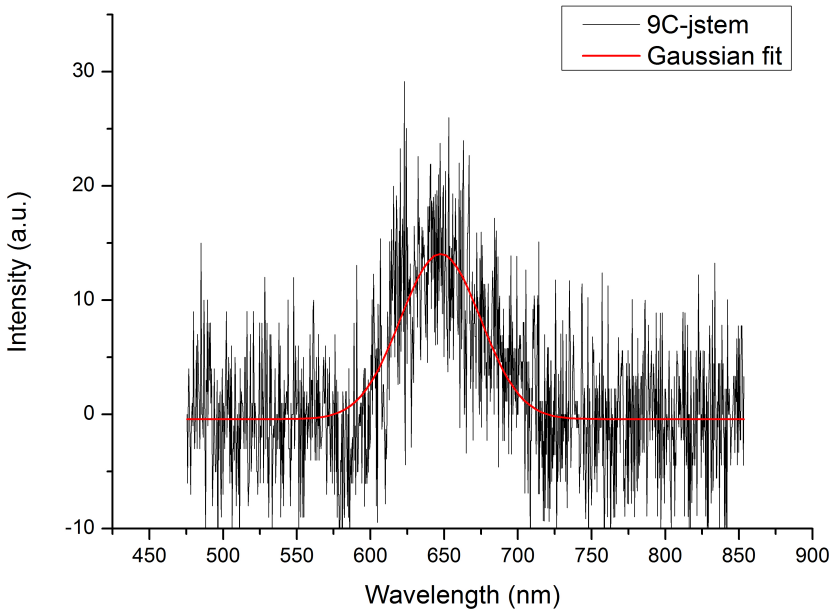

Figure 3.1: *Emission spectrum of a single 9C-hairpin emitter at room temperature, for 580nm excitation. Emission below* $\sim 610nm$ *is filtered by emission filters and the dichroic mirror. The red line is a Gaussian fit of the data.*

Figure 3.1 shows an emission spectrum from an individual 9C-hairpin emitter at room temperature. For these measurements, the stem of the hairpin was identical to the one attached to the modified DX-tubes (known as the 'jstem'). The Gaussian fit shows a FWHM of $64\text{nm} \pm 3\text{nm}$ around a 648nm peak. Single emitters have been shown to have emission spectra differing from emitter to emitter [5], but the 9C-jstem emitter's spectral properties are not noticeably different from those of 9C-hairpins with different stems.

Spectral measurements on the emission of larger collections of individual hairpin-emitters have been made to observe spectral width and emission intensity from an ensemble of independent

emitters. A large concentration of hairpins was spin-cast onto the substrate to allow multiple emitters to be excited at once by the laser beam.

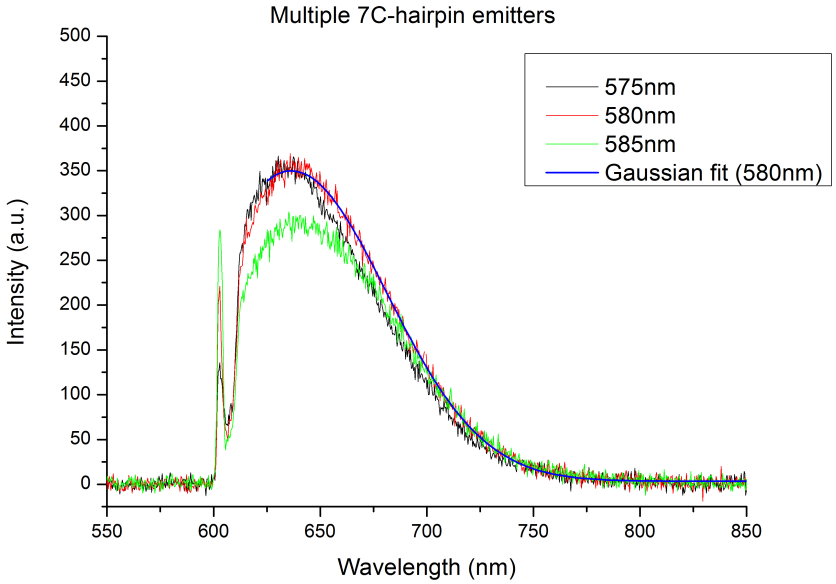

Figure 3.2: *Emission spectra of multiple individual 7C-hairpin emitters for 575nm (black), 580nm (red) and 585nm (green) excitations, taken at room temperature. The concentration used was 200nM, allowing many emitters to be excited at once. The unusual behavior for wavelengths below ∼610nm is due to the influence of emission filters and dichroic mirror. The blue line is a Gaussian fit of the 580nm data.*

The slight spectral variation between the emissions for different excitation wavelengths is due to the presence of individual emitters with slightly different absorption spectra. The Gaussian fit shows a FWHM of 100nm around a 638nm peak, which is consistent with a large quantity of spectrally slightly different individual emitters contributing individually to the emission.

3.2 7C-/9C-hairpin emitters on DX-nanotubes

3.2.1 Spectral properties

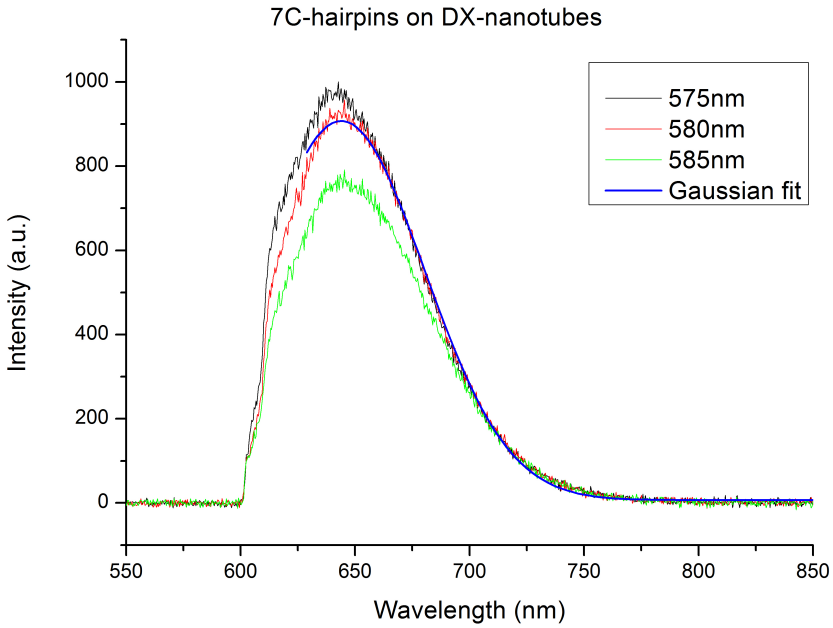

Figure 3.3: *Emission spectra of 7C-hairpin emitters on DX-nanotubes, at room temperature. The blue line is a Gaussian fit of the data taken at 580nm excitation, corresponding to a 91nm FWHM around a 642nm peak. The intensity increases when the excitation wavelength is tuned towards the blue, and is highest for 575nm excitation. Emission below ∼610nm is filtered by emission filters and the dichroic mirror.*

Spectral measurements on 7C-tubes using the Single Molecule Spectroscopy-setup have produced the emission spectra shown in Figure 3.3. These measurements were made based on a sample with a 1.33μM concentration of hairpins. A Gaussian fit of the emission spectrum for 580nm excitation yields a 91nm FWHM around a 642nm peak, making it slightly narrower than the 100nm width of the emission spectrum of individual emitters in Figure 3.2.

3.2.2 Intensity

Whilst the intensity of individual (tangles of) tubes varies drastically from measurement to measurement, emission spectra show comparable overall intensities to those of relatively smaller collections of individual hairpins.

Each circumference of the tube consists of around 7 tiles, meaning there will be around 7 hairpins per circumference of the tube, and the length of the tiles is 14.3nm. Because of this, one would expect to be exciting hundreds of emitters with a focussed laser spot, based on the estimated chemical yield of 45% for the synthesis of emitters on these tubes that has been reported [4]. If multiple tubes tangle together, which is the case for these tube-structures when silver-clusters are synthesized on them, even more emitters would be excited by the laser.

Because the intensity of the emission from a collection of emitters on the tube is similar to that of the emission from a smaller number of individual emitters, an intensity comparison has been made between separate hairpin-based emitters (7C and 9C) and the same emitters on DX-nanotubes.

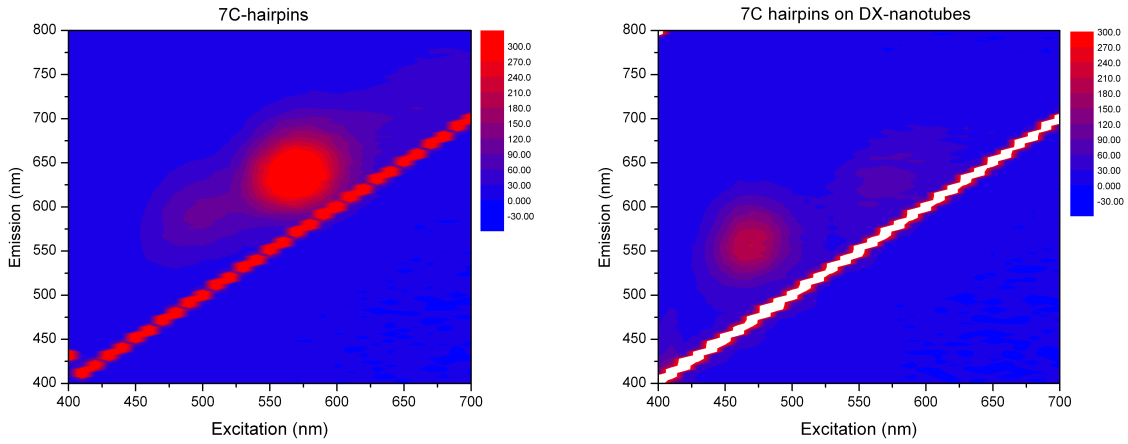

Figure 3.4: Fluorimetry of individual hairpins in solution (left), and of 7C-emitters on DX-nanotubes in solution (right). The concentrations were 2μM, and the used PMT voltage setting was 950V for both measurements. A red peak is present around 570nm excitation and 650nm emission, which is much more intense when the hairpins are not on tubes (left). The secondary peak around 480nm excitation is blue-shifted and more intense when the emitters are placed on tubes.

Figure 3.4 shows measurements of the overall intensity in the samples through fluorimetry. The red peak around 580nm-excitation is clearly much brighter for the individual emitters (by a factor of 5). The relatively blue peak has a reasonable intensity on the tubes, however, and it's shifted slightly further into the blue (∼465nm) than its usual position for single emitters (∼480nm). Because the measurements in this thesis are based upon the emission for excitations between 575nm and 595nm (the output range of the dye laser), this shows why the intensities in spectroscopy-measurements were lower than expected.

To determine whether the decreased overall intensity of the emission from the emitters on the tubes is the result of a lower chemical yield in the emitter-synthesis (meaning a lower overall quantity of fluorescent emitters), or of a lower average quantum yield per emitter when they are placed on tubes, the tubes were broken whilst the intensity was measured. This was performed by heating them up slowly to separate the individual tiles without breaking the hairpin structures.

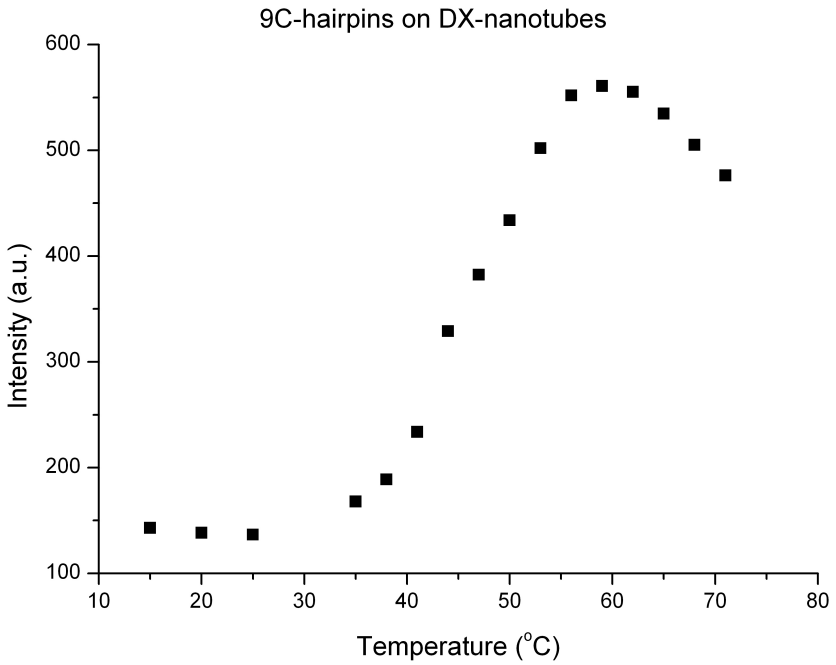

Figure 3.5: *Emission intensity of the 9C-nanotube sample, measured by fluorimeter, when the temperature of the solution is raised from 15°C to 71°C . Shown is the average intensity around the 640nm emission peak for 570nm excitation.*

When the temperature of the sample is increased, the 9C-nanotubes show an increase in total intensity by a factor of 4, before decreasing again when the temperature is increased above ~55°C. IDT software predicts that the hairpins will have a melting temperature close to 53°C. The melting temperature of the tube structure should be lower to ensure the strands anneal into tubes during tube-production, meaning the tiles should separate well before the individual hairpins start to break. The intensity behavior is consistent with an increased intensity when the tiles separate combined with a decrease for the breaking of individual hairpins.

3.2.3 Intensity time-traces

To see if there were any regularities in the behavior of the overall emission intensity of an ensemble when it is excited in the Single Molecule Spectroscopy Setup, time-traces were taken of the emission gathered from the emitters in the laser spot. The measurement was 25 minutes long to allow the relatively large emitter-ensemble to photobleach almost fully, so that all the relevant information had been gathered.

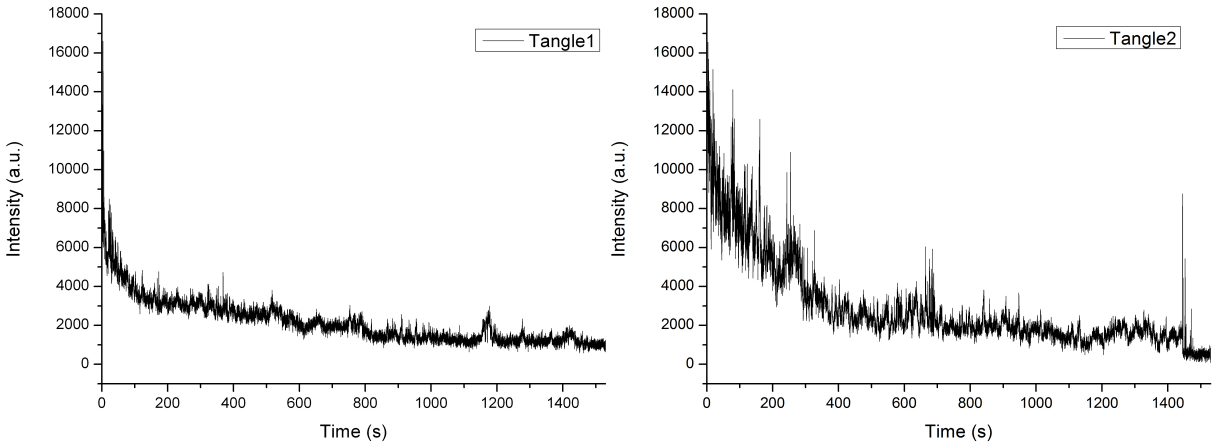

Figure 3.6: *Intensity time-traces of the emission from 9C-hairpin emitters on two tangles of DX-nanotubes. Data-points are produced at 100ms intervals. The graphs show blinking behavior in the intensity of the emission in the form of steps, and an overall decay with time due to photobleaching of the individual emitters.*

The intensity time-traces show an overall decay due to the photobleaching of the individual emitters, combined with rapid on-and-off behavior due to blinking of the individual emitters in the ensemble. When a large concentration of emitters is present, an increased amount of stray light makes the background vary between measurements performed on different parts of the substrate. As a result, the background is difficult to characterize for different measurements, which is why the measured intensities do not go down to zero completely.

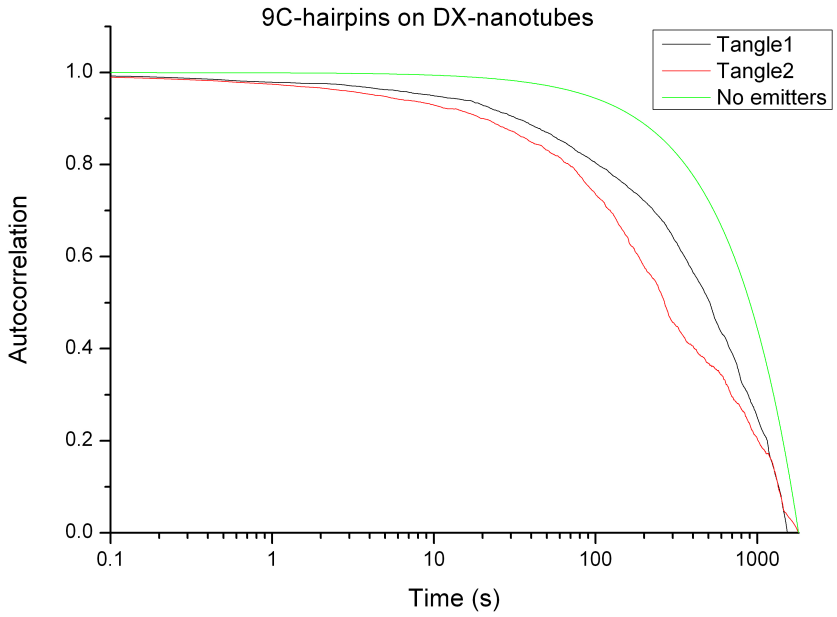

Figure 3.7: *Autocorrelation function based on the data shown in Figure 3.6. The green line is the autocorrelation function of a measurement on the background noise.*

No particularly large peaks are visible in the autocorrelation function of the time-traces made of the 9C-tubes. The decay rates are ill-defined because the level of the background varies from measurement to measurement.

3.2.4 Discussion

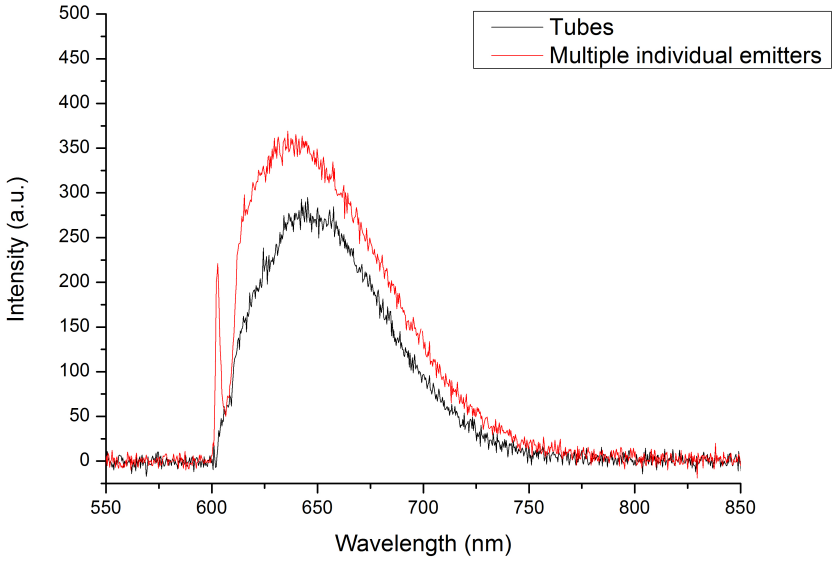

Figure 3.8: *Emission spectra of 7C-emitters on DX-nanotubes (black), and of a large concentration of individual emitters (red). The excitation wavelength was 580nm. The spectral shape for emission below $\sim$ 610nm is influenced by emission filters and the dichroic mirror.*

Spectral properties

A slight blue shift in the emission from emitters on tubes relative to the emission from an ensemble of individual emitters has been reported for emitters on DX-nanotubes [4]. This blue-shift does not seem to be present in our measurements. The shape of the emission spectra is a Gaussian for both cases. The measured intensity of the emission from the collection of individual emitters is higher than it is for the emission from the emitters attached to the DX-nanotubes.

Intensity

Figure 3.5 shows an increased emission from a batch of DX-nanotubes containing fluorescent emitters when the temperature is raised, leading to a maximum intensity between 4 and 5 times higher than at room temperature.

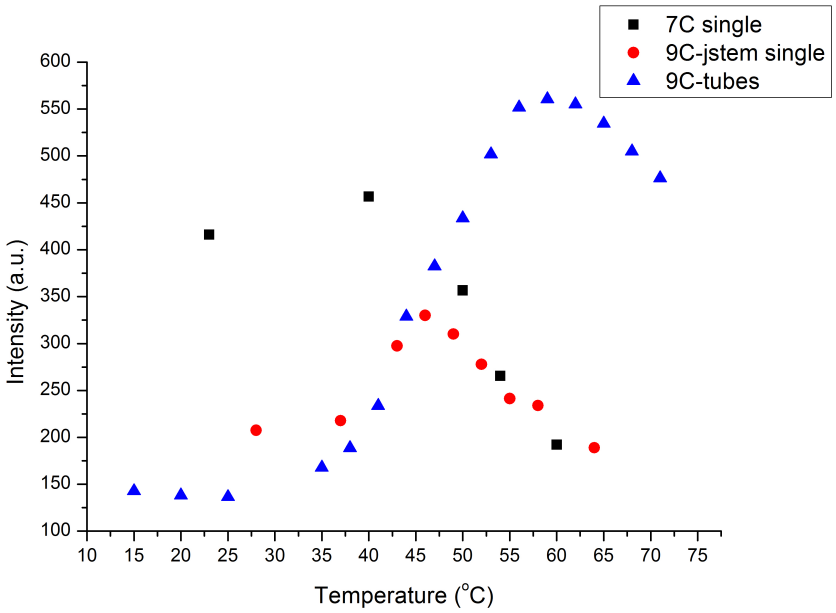

Figure 3.9: *Average emission intensities of separate 7C- and 9C-hairpin emitters vs 9C-hairpins on DX-nanotubes, when the temperature is raised. The stem of the hairpins has been matched for both 9C-cases.*

Figure 3.9 shows the different behavior of the emitter ensembles when the temperature is raised. Generally, the overall emission from individual emitters will decrease when the temperature is raised, as seen in the 7C-hairpin behavior. When the 'jstem' is the stem of the hairpins, the emitters show a slightly increased intensity similar to the behavior when the emitters are on the DX-nanotubes, before decreasing again when the temperature is raised above 45^{o}C.

This decrease in the emission from the emitters when they are on DX-nanotubes can either be the result of an emitter-emitter interaction quenching the intensity, or of the change in environment when the emitters are placed on the DX-nanotube. The 9C-hairpins will have a 3nm circumference, meaning that, although the exact configuration of the silver cluster and of its encapsulation are largely unknown, a 10-atom large cluster could have room to move around. Additionally, as is illustrated in Figure 1.4, the loop containing the silver cluster is designed to be close to the tube structure. It is therefore possible that the DX-nanotube structure is applying a force onto the silver cluster due to its close proximity, causing the cluster to move out of its optimal position within the hairpin. Breaking the tubes would then remove this force, allowing the silver clusters to regain emission intensity.

A notable point of interest, however, is the lack of this decreased intensity-effect for the blue-shifted strain of emitters present in the sample, as seen in the fluorimetries in Figure 3.4. This means that either

i) The 'blue' emitters are structurally different in such a way that they do not suffer the same effect from the presence of the tube, or

ii) A lower overall concentration of the emitters emitting at these shorter wavelengths, resulting in larger emitter-emitter distances, does not allow quenching to occur between these emitters on the tube.

Interference from the tubes can't be present for the individual 9C-hairpins, however. The main difference between the 'jstem' and other stems, such as the one used for the 7C-comparison in Figure 3.8, lies in its length. A longer stem means there are more basepairs contributing to the rigidity of the structure, meaning the encapsulation can be of a different nature as well. If this

causes the cluster to be confined in such a way that it cannot be in its optimal configuration, the small increase in intensity can be the result of the sequential breaking of single base-pair bonds within this stem, allowing the encapsulation to change, before the structure breaks completely.

Of course, this second explanation can also be applied to the emitters on tubes. This is made less likely, however, due to the tiles being relatively rigid structures that are designed to have a higher melting temperature than the tube structure itself. Whilst the tiles could induce an increased tightening of the encapsulation as well, one would expect the increase in intensity to occur at a significantly higher temperature than for the individual emitters.

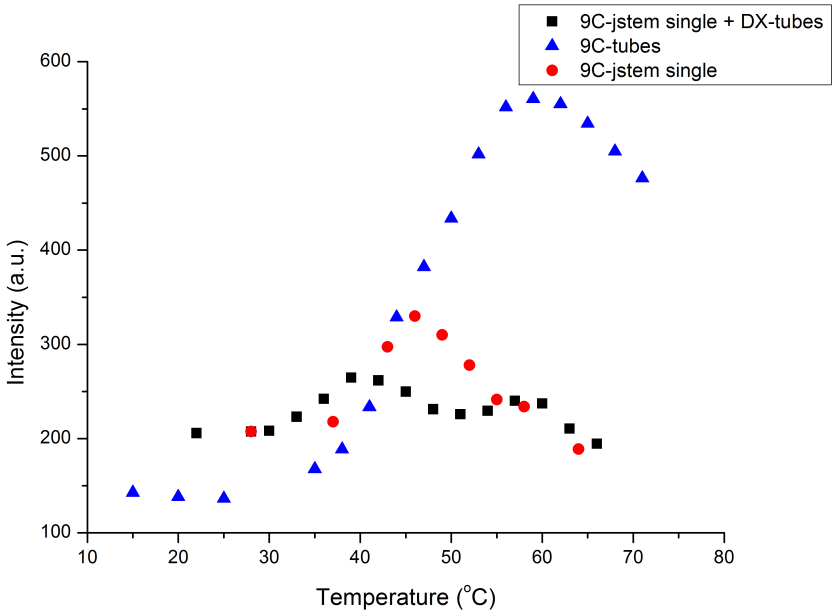

Figure 3.10: *Comparison between 9C-jstem individual emitters (red dots), 9C-jstem individual emitters in solution with DX-nanotubes (black squares), and 9C-jstem emitters attached to DX-nanotubes (blue triangles), as a function of the temperature of the solution. The shown intensities are average emission intensities around the emission peak, for 570nm excitation.*

To investigate the environmental effects on the emission from individual hairpin-emitters when they are in solution with DX-nanotubes, individual fluorescent 9C-emitters were added to a solution of annealed DX-nanotubes. As shown in Figure 3.10, this not result in the same behavior when the temperature of the solution is increased. This means that the decreased intensity for the emitters when they are placed on DX-nanotubes is not the result of environmentals introduced when the tubes are produced, such as loose DNA-strands or other chemical differences. A small second peak around 58°C introduced into the intensity behavior when compared to the small increase in intensity of the 9C-'jstem' single emitters, however, indicating that some of the hairpins may 'stick' to the tube structure, causing an increased intensity in the emission from these emitters when the tubes break.

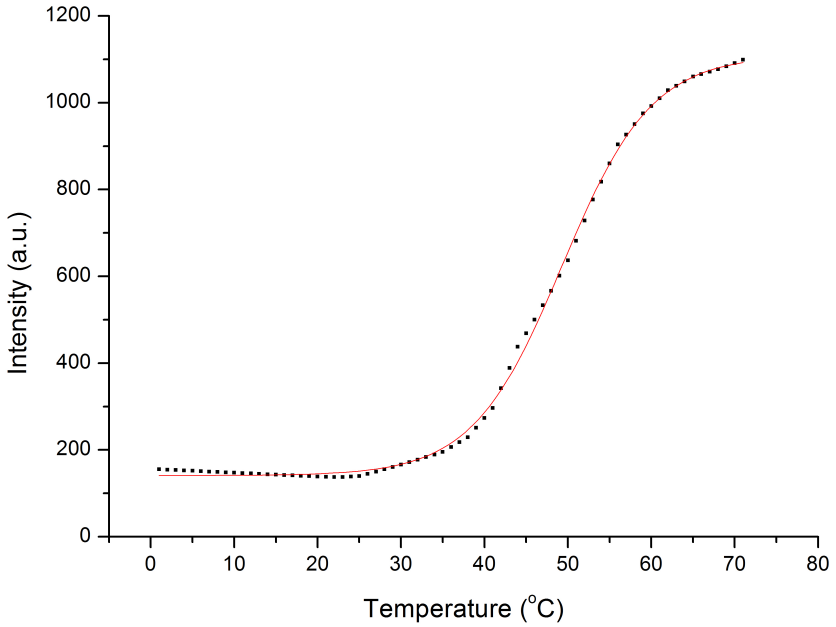

Figure 3.11: *Intensity of the emission from 9C-hairpin emitters on DX-nanotubes as shown in Figure 3.5, with the decay in intensity due to the breaking of individual hairpins factored out. The red line is a sigmoidal fit of a Boltzmann distribution-based ensemble, indicating relative emission intensities of 160 a.u. and 1305 a.u. before and after the tubes are broken, respectively.*

Figure 3.11 shows an estimated behavior of the intensity of the emission from emitters on DX-nanotubes, while factoring out the decreased fluorescence due to the breaking of hairpins. A linear interpolation of the data in Figure 3.9 has been made. The behavior from individual emitters as a function of temperature is factored out, leaving a translation along the temperature-axis as a variable, and the ensemble is made to fit a Boltzmann-distribution. The Boltzmann-fit leads to an estimated decrease in intensity for the hairpin-emitters by a factor of 8.1 when they are attached to DX-nanotubes, and a melting temperature of the tubes of 48.7^{o}C.

This procedure assumes that all the DX-nanotubes will be broken at temperatures above 65^{o}C, so that the decay in the emission intensity from the emitters on these tubes (Figure 3.9, blue triangles), can be completely attributed to the breaking of individual emitters in this temperature range. Because of this, the unusual behavior in the emission from 9C-'jstem' individual emitters as a function of temperature (Figure 3.10) is neglected.

Intensity time-traces

The behavior of the intensity of the emission from the ensembles of hairpin-emitters on DX-nanotubes (Figures 3.6 and 3.7) show blinking of individual emitters on the tubes, and a gradual photobleaching of emitters in the ensemble. The autocorrelation function shows no peaks that would point to fixed timescales in the blinking or bleaching behavior of the ensemble, which is consistent with a large bunch of individual emitters operating within their own time-frame. If large collections of emitters were interacting on the tube, one would expect to see a more coherent behavior in the emission of these emitters, leading one to believe that the there are no ensemble-wide interactions between the emitters. This agrees with the lack of any different spectral shape for the emission from the emitters on the tube (no dips, narrowing, asymmetry), and makes the environmental reasoning behind the decreased average quantum yield, as seen in the emission intensity under temperature variations, more likely. Smaller interactions between pairs, triplets or other small collections of emitters would be disguised by the large quantity of emitters, however.

Chapter 4

Silver clusters on 6HX-nanotubes

4.1 Modified 6HX-nanotubes

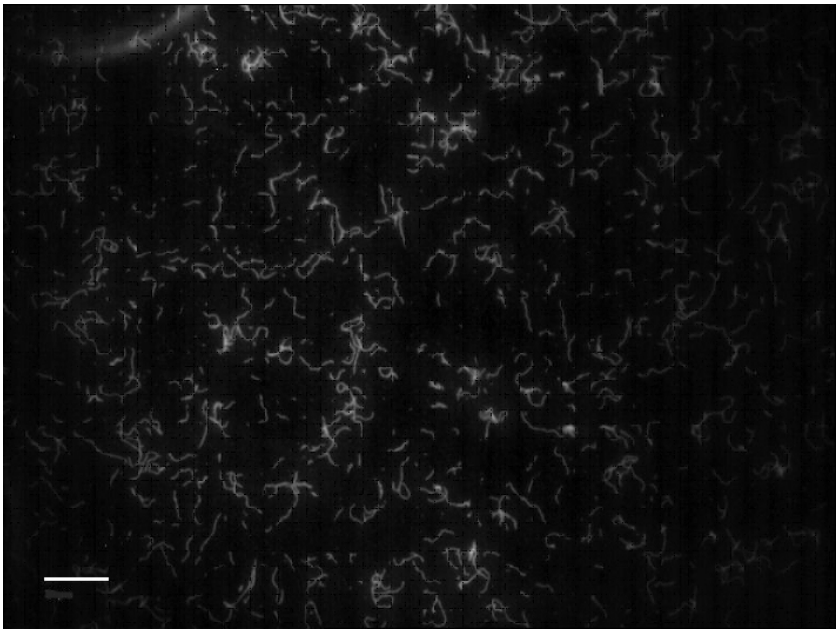

Figure 4.1: *Image of 6HX-nanotubes produced by fluorescence microscopy. The tubes are made visible by the fluorescence from Cy3-dye molecules attached to the 5'-ends of the U1-strands. The concentration of the sample was 20nM. The scale bar represents 10μm in length, meaning the tubes are around 6μm in length on average.*

The production process as described in section 2.1.3 was effective in producing 6HX-nanotubes, as is shown in Figure 4.1. A reasonable volume of tubes is produced, the average length matching the 6μm expected from original experiments with these tubes [8].

In order to allow formation of fluorescent silver clusters on the 6HX-nanotubes, multiple modifications to the tube structure have been tried. Modifications were limited to the 5'-end of the U3-strands and the 3'-end of the U5-strands in order to place the clusters in close enough proximity to allow possible FRET-interactions with the Cy3 on the 5'-end of U1 as a donor.

4.1.1 'Rockstar'

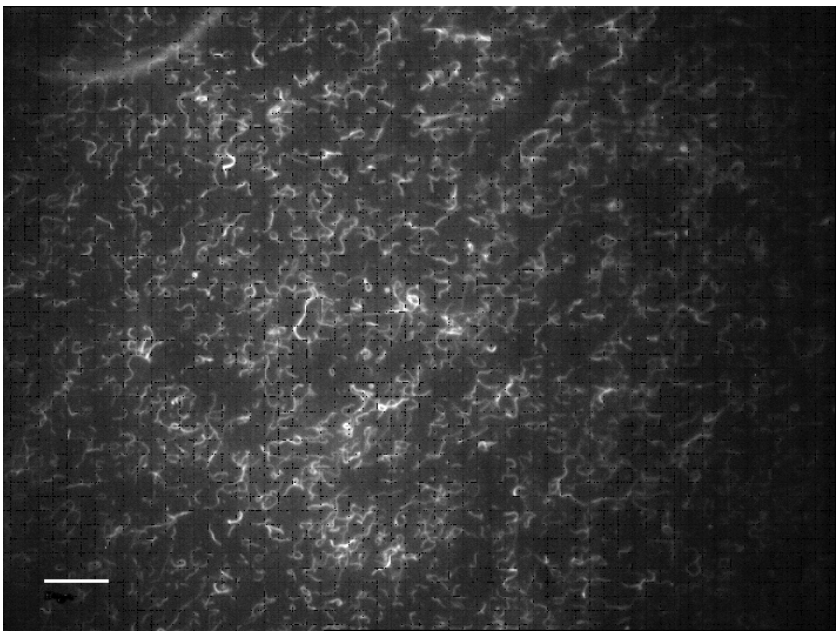

Figure 4.2: *Image of 6HX-nanotubes, modified through addition of a 'Rockstar'-strand to the 5'-end of the U3-strand. The tubes are made visible by the fluorescence from Cy3-dye molecules attached to the 5'-ends of the U1-strands. No silver has been added. The concentration of the sample was 30nM. The scale bar is 10μm, meaning the tubes are around 6μm in length on average.*

Adding a 'Rockstar'-strand to the 5'-end of the U3-strands does not disturb the annealing process appreciably. A similar concentration of separate tubes are produced as was the case for unmodified tubes, as shown in Figure 4.2. The same modification was tried on the 3'-end of the U5-strand, but this does not seem to allow the tubes to be produced reliably.

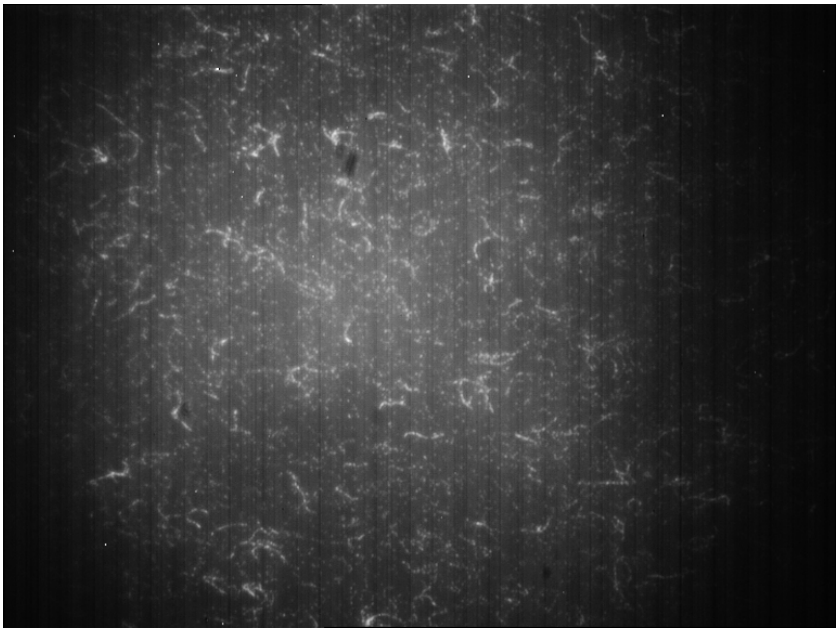

Figure 4.3: *Image of 6HX-nanotubes, modified through addition of a 'Rockstar'-strand to the 5'-end of the U3-strand, after silver cluster synthesis. The Cy3-dye is not present in this sample. Tube length and concentration seem similar to the image taken before silver cluster synthesis (Figure 4.2). Individual emitters, or small collections thereof, are visible as dots on the tubes.*

Figure 4.3 shows 6HX-nanotubes with 'Rockstar'-emitters attached to the 5'-end of the U3-strands. The intensity is low, but the tubes are visible under the fluorescence microscope. Individual emitters, or small collections thereof, can be discerned on the tube, indicating a relatively low chemical yield of visibly fluorescent emitters forming on the 'Rockstar'-strands.

The image has been taken 3.5 hours after addition of $NaBH_4$. Generally, Ag:DNA's become fluorescent almost immediately, but the intensity of the emission that can be collected from a batch of emitters will increase gradually to a maximum after around 15 hours. The intensity measurements shown in Figure 4.4 indicate that this is the case for the 6HX-'Rockstar'-tubes as well. The visibly low emitter yield on the tubes agree with this assessment: There may be more strands containing silver clusters on the tubes, but they may not yet show enough fluorescence to be seen.

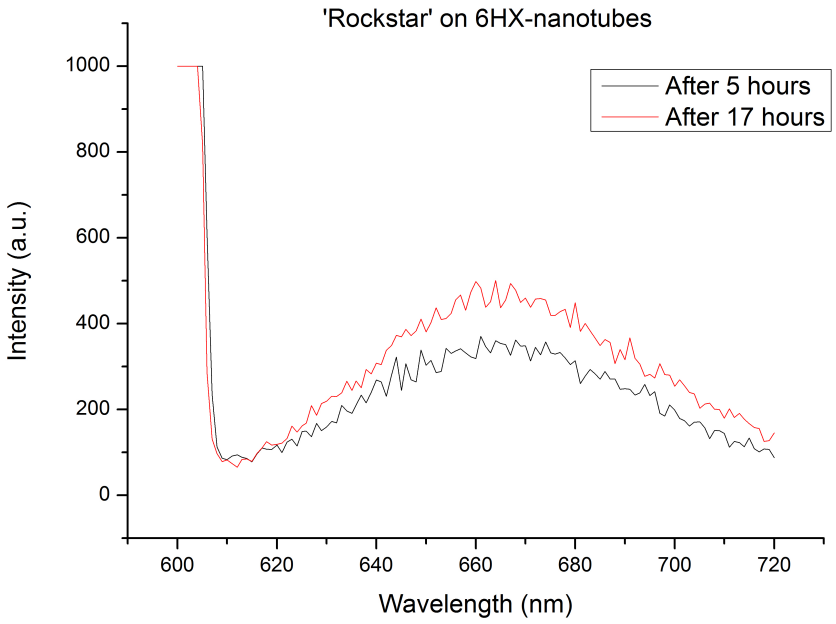

Figure 4.4: *Spectroscopy of 6HX-'Rockstar' tubes, taken with the tubes in solution through use of the fluorimeter, after 5 hours (black) and after 17 hours (red). The excitation wavelength was 600nm, producing maximum emission in both cases.*

Whilst the overall intensity of the sample increases, however, the visibility of the individual tubes decreases drastically when they are viewed more than 6 hours after the reduction, making the tubes impossible to examine through fluorescence microscopy. When they are excited by laser and detected by the CCD-camera in the Single Molecule Spectroscopy-setup, the tubes remain visible for a short time, with a large portion of the emitters bleaching within 30 seconds. This rapid photobleaching is the probable reason for their lack of visibility under the fluorescence microscope. Because of this, all measurements discussed in this thesis are made with the tubes in a similar condition to the ones shown in Figure 4.3, i.e. 3-4 hours after addition of the reducing agent.

4.1.2 9C-hairpins

In an attempt to attach other emitters to the 6HX-nanotubes, 9C-hairpins were added to the strands as well. The produced samples showed an increased risk of the strands clumping together to form larger random structures. Figure 4.5 shows that, whilst a relatively low yield of tubes can still be obtained, larger irregularities are introduced into the system. Unlike addition of the 'Rockstar'-strand, modifying the 3'-end of the U5-strand in this way produced better results than modifications to the 5'-end U3-strand.

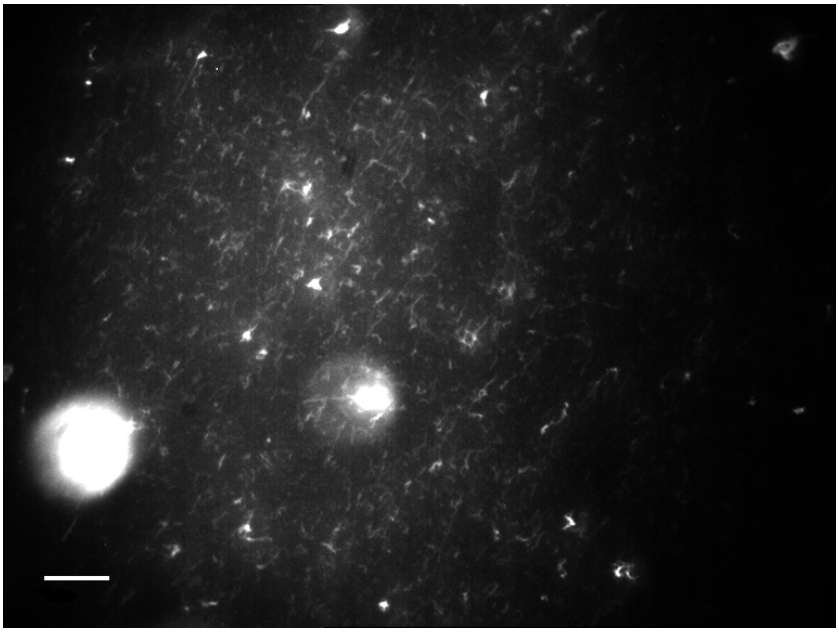

Figure 4.5: *6HX-nanotubes with a 9C-hairpin added to the 3'-end of the U5-strand. The concentration of the sample was 150nM. The tubes are clumped together in places, and seem to be shorter in length.*

4.1.3 Universal attachments

Attaching the emitters to the fully annealed 6HX-nanotubes has also been attempted. To accommodate this, an addition has been made to the U3- or U5- strands in the form of a 10-base 'tail' of thymines and adenines (5'-ATT-ATA-ATT-T-3'). These bases should be relatively inert with regard to stabilizing fluorescent silver clusters. Attaching the emitters afterwards would allow observing the annealing of the tubes and the synthesis of the emitters processes separately, before combining the two products. Advantages would be the potential for an increased chemical yield of the emitter synthesis when it is performed separately, and a clear before-and-after picture of the changes the emitters undergo after being placed on the DNA-tubes.

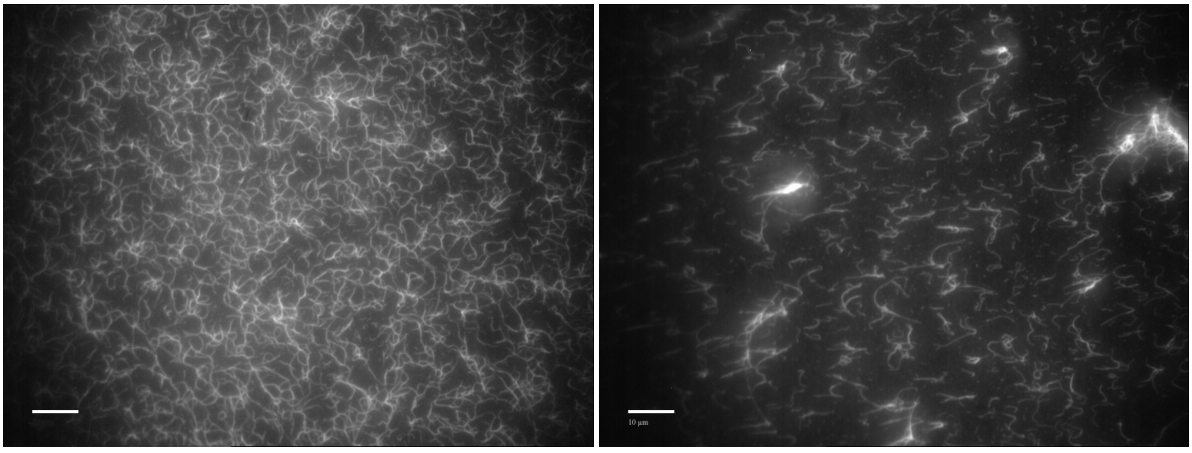

Figure 4.6: *6HX-nanotubes with a 'tail'-addition to the 5'-end of the U3-strand (left) and to the 3'-end of the U5-strand (right). Sample concentrations were 300nM for both images. Modifying the 5'-end of the U3-strand produces a similar result to the un-modified tubes (Figure 4.1). When the 3'-end of the U5-strand is modified, a smaller concentration of tube-like structures are present.*

As has been seen with the 'Rockstar'-strands, modifying the 5'-end of the U3-strand through addition of the 'tail' does not seem to disturb the annealing process at all (Figure 4.6). Modifications to the 3'-end of the U5-strand produces a much smaller concentration of tubes and larger structures, combined with larger clumps of strands.
Attempting to attach the 'Rockstar' using these methods has not produced the desired results. Through observation of the individual emitters under the fluorescence microscope, it has been confirmed that the emitters are not attached to a tube-structure. Unfortunately, the signal from individual emitters is too low for imaging to be effective. From this we can deduce, however, that the 'tail'-addition to the 'Rockstar'-strand becomes involved with the encapsulation process, causing it to no longer be (reliably) available for tube-attachment.

An attempt has been made to attach 9C-hairpin emitters to the 6HX-nanotube structures using the same process.

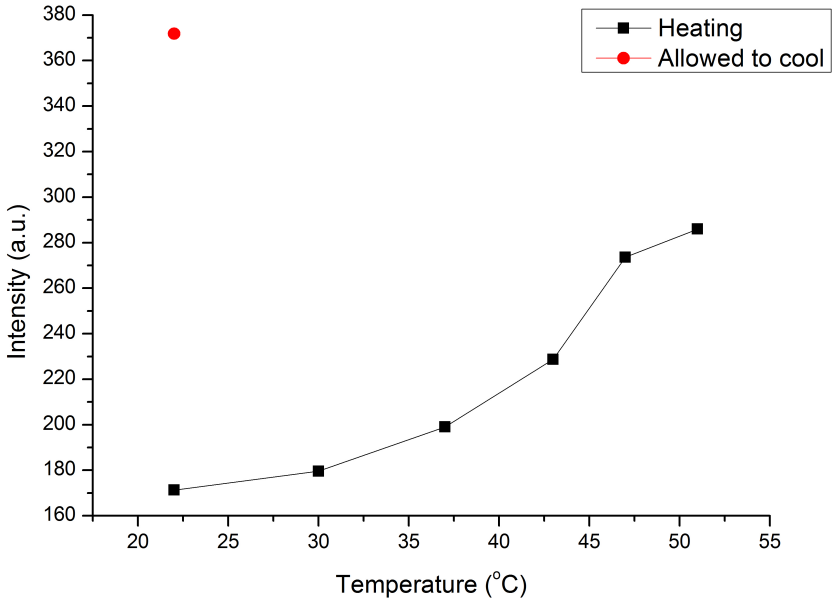

Figure 4.7: *Average emission intensity of the emission from 9C-hairpins with 'tail' addition added to matching 6HX-nanotubes, as a function of the temperature of the solution. The sample was excited by 570nm light.*

Figure 4.7 shows intensity measurements on 9C-emitters when the attempt has been made to attach them to 6HX-nanotubes using 'tail'-modifications. The overall increase is quite small, around a factor 1.7 from 25-58°C. There are two chemical yields involved in deciding the density of emitters on the tube structure, the chemical yield of the synthesis of the individual fluorescent silver clusters, and that of the attachment of the already fluorescent emitters to the tube. The relatively small increase in intensity can be thebut the presence of the emitters on the 6HX-nanotube structure is likely, if not completely confirmed.

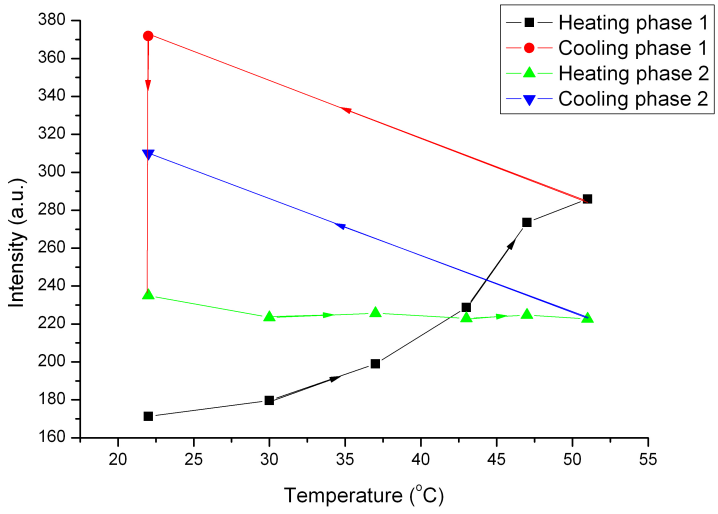

Figure 4.8: *Average intensity of 9C-hairpins with 'tail' addition added to matching 6HX-nanotubes. The temperature is raised (black arrows), causing the intensity to increase. When the sample is allowed to cool down (red arrows), the intensity increases further during cooldown (red dot), but is decreased after 3.5 hours. Re-heating the sample (green arrows) causes the sample to maintain its intensity, and cooling down (blue arrows) increases the intensity again. The sample was excited by 570nm light.*

Figure 4.8 shows repetition of a heating-cooling process on the 6HX-nanotubes after attempted attachment of the 9C-hairpin emitters. When the sample is heated, the hairpins, if attached, will become separated from the tube, the 'tails' being the most likely breaking point, because they consist of 10 base-pairs compared to 42 per tile for the tube structure. When the solution is heated to51^oC, and allowed to cool down to room temperature, the intensity of the emission increases to indicate the emitters becoming separated from the tubes, by a factor of 2.1. If the sample is given a few hours to settle, the intensity will decrease again, which points towards re-attachment of the emitters to the tube-structure. Heating the solution up again and allowing it to cool down increases the intensity by a factor of 1.4, indicating that some of the individual emitters and/or tubes have been broken by the first heating cycle.

4.2 Individual 'Rockstar' emitters

The emission spectra of individual 'Rockstar'-emitters were taken from 'Rockstar'-samples based on strands including the 'tail'-attachment mentioned section 4.1.3, to the 3'-end. When the emitters are made part of the 6HX-nanotube structure, the 'Rockstar'-strand will be attached on the 3'-end as well. Measurements have been made on these emitters to characterize their spectral properties, overall intensity of emission and the intensity behavior over time, for use in a comparison with 'Rockstar'-emitters on 6HX-nanotubes.

4.2.1 Spectral properties

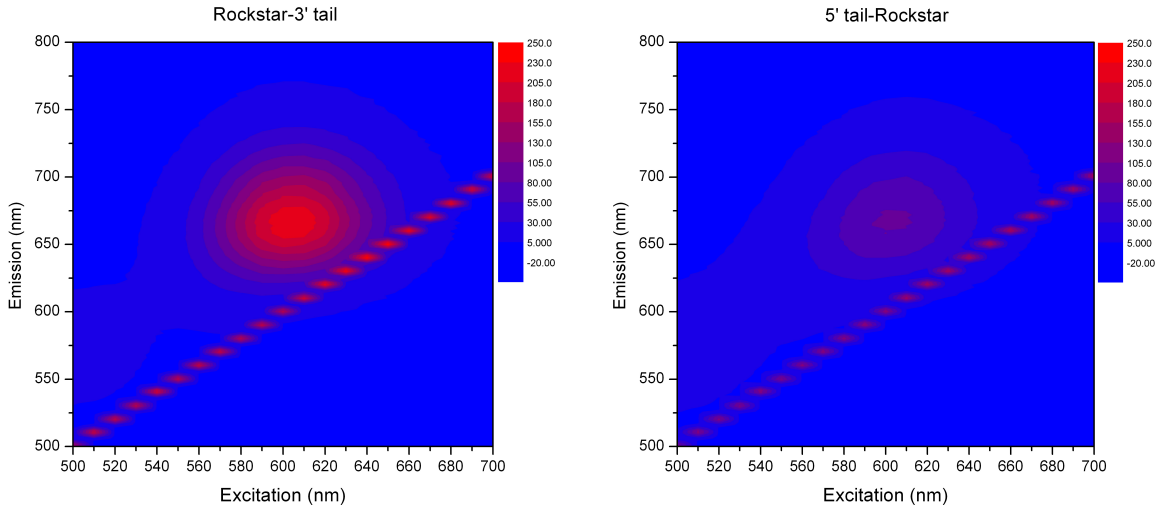

Figure 4.9: *Fluorimetry of 'Rockstar'-emitters with modified 3'- (left) or 5'-ends (right). The emission is centered around 660nm for a 600nm excitation in both cases. The 'Rockstar'-emitters with modified 3'-ends show a significantly higher emission intensity than those with modified 5'-ends.*

Modifying the 3'-end or the 5'-end in this way resulted in a large difference in optical properties. The red emission peak that is centered around 600nm excitation shows significantly less intensity when the 5'-end is modified through addition of the 'tail'. This may mean that the 5'-end of the 'Rockstar'-strand is more involved in forming the encapsulation. Because of this, and because of better chemical- and/or quantum yields when synthesizing this emitter as evidenced by the fluorimetries in Figure 4.9, the 'Rockstar'-3tail strand was used for measurements involving individual emitters.

The 'Rockstar'-ensemble is centered around a peak further into the red than the emission produced by 7C- or 9C-hairpins.

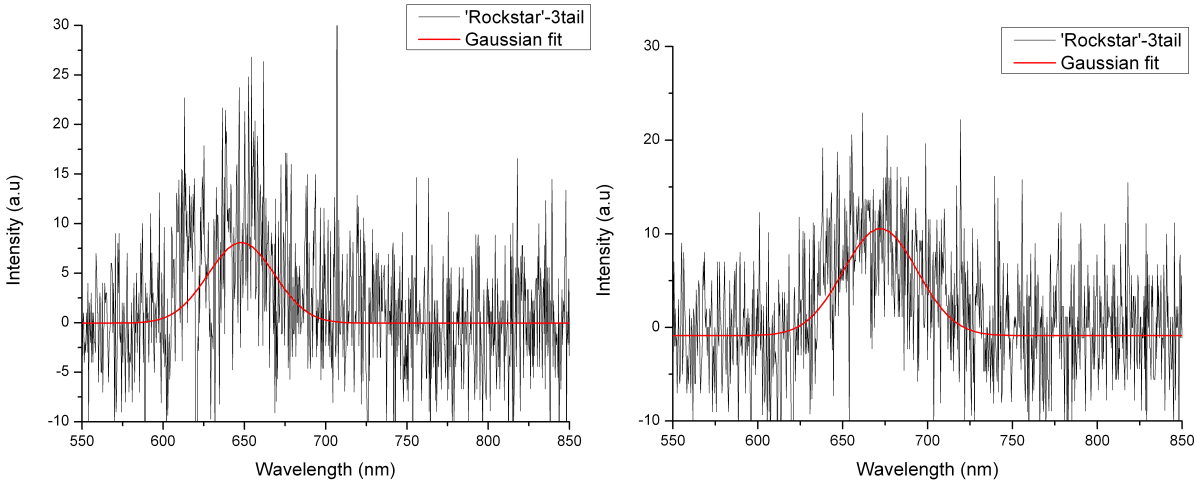

Figure 4.10: *Room temperature spectrum of a 'Rockstar'-3tail single emitter for 595nm excitation. The red lines are Gaussian fits of the data made to show the relative probable peak-positions.*

Single emitter spectroscopy can be performed on the single 'Rockstar'-3tail emitters at room

temperature, though it yields relatively low signal-to-noise ratios, as is evident in Figure 4.10. The Gaussian fits of the measurements are relatively ill-defined because of the noise, but can be used to determine the most likely peak-positions, and estimate the spectral widths. For the first (left) emitter, this yields a FWHM of 48nm $\pm$11nm around a 648nm emission peak. The second (right) emitter has an estimated FWHM of 47nm $\pm$12nm around 668nm.

4.2.2 Intensity

The intensity of the emission from a collection of 'Rockstar' individual emitters in solution was measured, while the temperature of the solution was raised (Figure 4.11). Because it is unknown how the encapsulation is formed for non-hairpin strands such as the 'Rockstar', it is not possible to predict under which conditions the individual encapsulations will break.

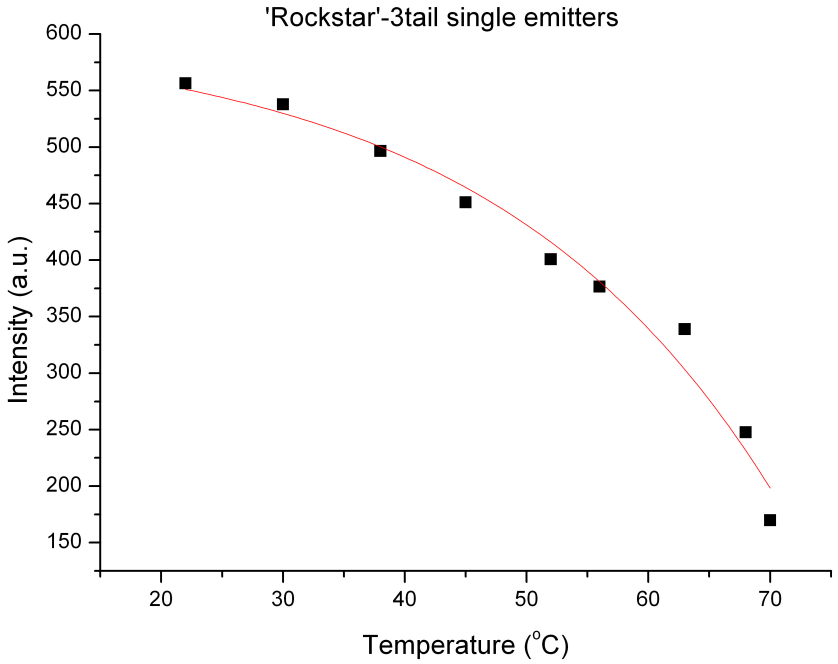

Figure 4.11: *Emission intensity of 'Rockstar'-3tail emitters in solution as a function of temperature, measured by fluorimeter. Shown is the average intensity around the emission peak for 600nm excitation. The red line is there to guide the eye and indicate an increasing rate of intensity decrease.*

4.2.3 Intensity time-traces

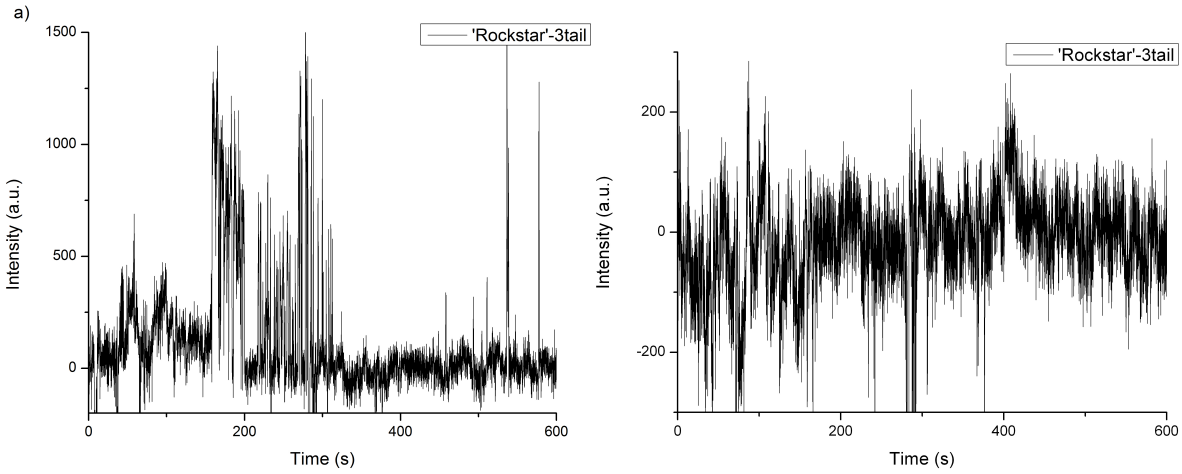

Figure 4.12: *Intensity time-traces taken from two individual 'Rockstar'-3tail emitters, at room temperature. The excitation wavelength was 595nm. Sharp steps in the intensity indicate blinking behavior of the emitter. The background is subtracted using a measurement taken from an emitter-less part of the substrate.*

Intensity time-traces of single 'Rockstar'-3tail emitters show varying levels of activity. Generally, at room temperature and in air, a reasonable amount of blinking activity can be observed (Figure 4.12a), and the emitters will be 'off' for a large portion of the time in which they are being excited. This behavior is consistent with reported measurements performed on Ag:DNA's under these conditions [5].

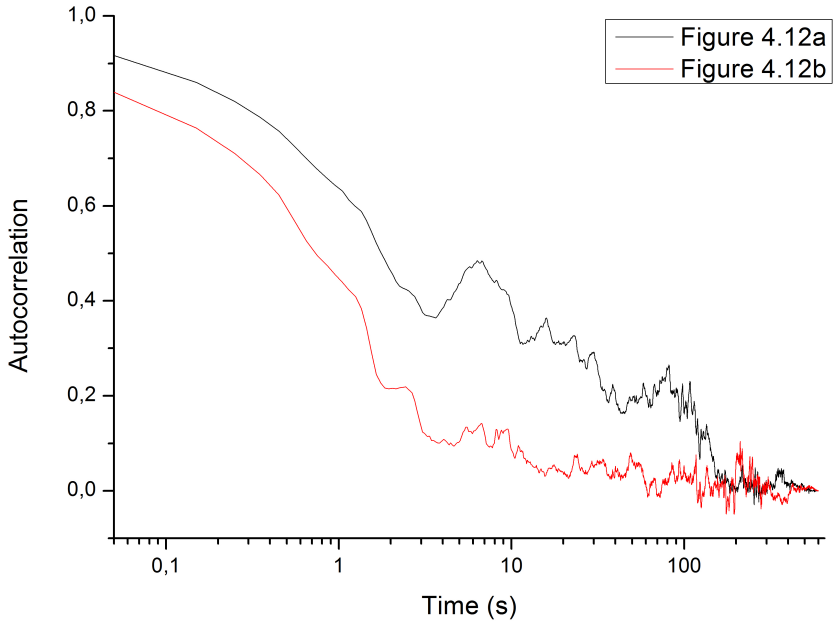

Figure 4.13: *Autocorrelation function of the data shown in Figure 4.12. The autocorrelations in the time-trace of the emitter in 4.12a show a noticeable broad peak around 6.7 seconds, and a collection of peaks in 80 second region.*

Peaks in the autocorrelation function can be found for single emitters that show significant blinking activity, as shown in Figure 4.12a. The peak that is present on the short timescale (6.7 seconds) can be attributed to the time between the individual 'on' and 'off' blinks in the emission. The longer timescales show less pronounced, broader collections of peaks which indicate consistencies in the timing of the appearance of collections of these shorter blinks.

4.3 'Rockstar' emitters on 6HX-nanotubes

All measurements on the 6HX-'Rockstar' tubes are made on 6HX-tubes modified through addition of a 'Rockstar'-strand to the 5'-end of the U3-strand. The spectral properties, overall intensity and the intensity behavior over time have been observed to facilitate a comparison with single 'Rockstar'-emitters.

4.3.1 Spectral properties

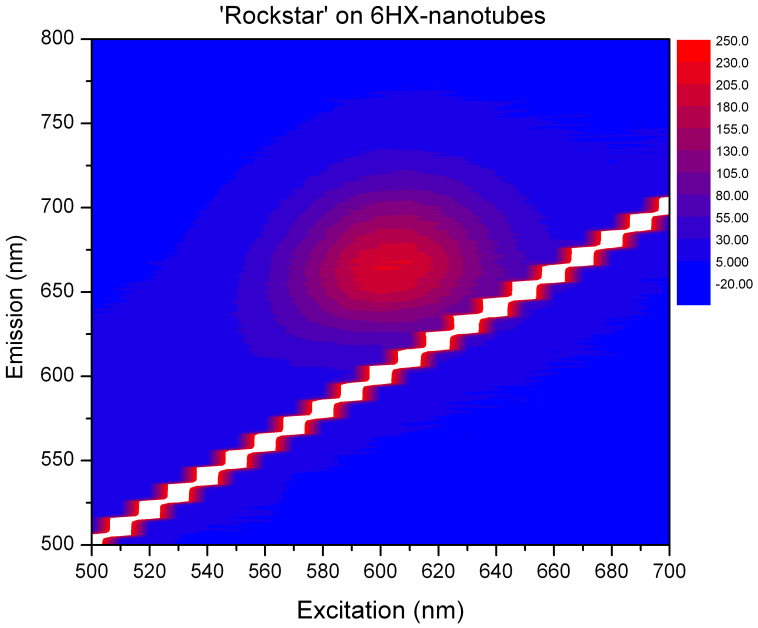

Figure 4.14: *Fluorimetry of 6HX-nanotubes with 'Rockstar'-emitters formed on them. The peak position and spectral characteristics are the same as for the 'Rockstar'-3tail single emitters (Figure 4.9). When the emission intensities are expressed in the same units, there is a 3 to 5 times higher emission intensity from a individual emitter-sample of the same concentration.*

Fluorimetry of the 'Rockstar'-emitters on 6HX-nanotubes has been performed to show that the maximum absorption- and emission-wavelengths of the emitters have not changed significantly. The emitters on the tubes show a maximum emission intensity 3 to 5 times lower than the emission from a 'Rockstar'-3tail sample of the same concentration.

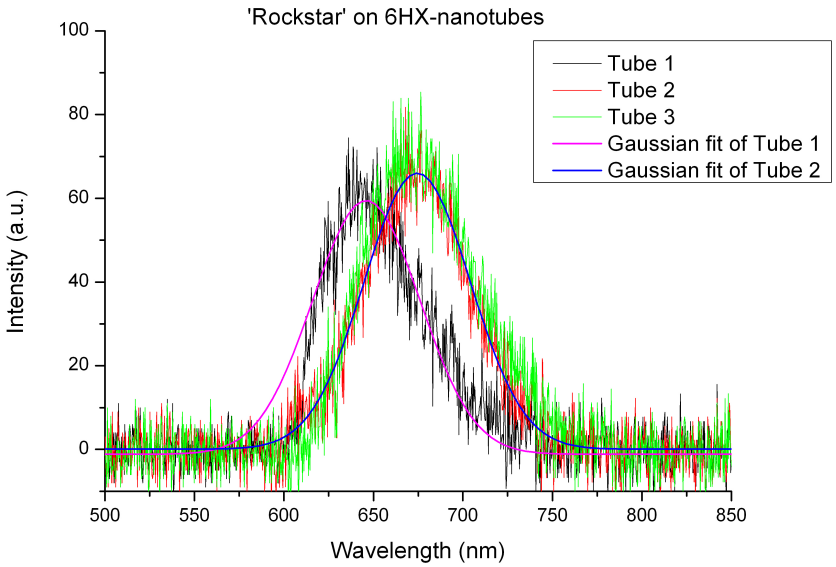

Figure 4.15: *Room temperature spectra of 'Rockstar'-emitters on three individual 6HX-nanotubes. Magenta and blue lines show Gaussian fits of the emission spectra from two tubes, referred to as 'Tube 1' and 'Tube 2'. Behavior for wavelengths below 610nm is filtered by the emission filters and dichroic mirror. The fits yield a 71nm FWHM around a 646nm peak and a 70nm FWHM around a 674nm peak for 'Tube 1' and 'Tube 2' respectively.*

Spectroscopy of the emission from 'Rockstar'-emitters on single 6HX-nanotubes yield spectra like the ones shown in Figure 4.15. Gaussian fits show a FWHM of 71nm around a 646nm peak for the relatively low-wavelength spectrum (Tube 1), and a FWHM of 70nm around a 674nm peak for Tube 2. Other measurements on these tubes show similar Gaussian spectra of similar widths with various peak-positions, similar to the spectral diversity in single emitters.

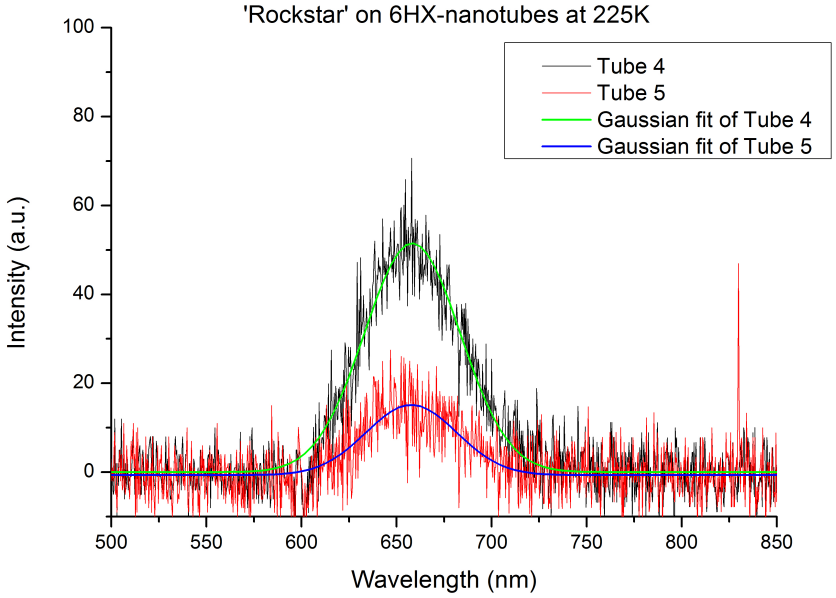

Figure 4.16: *Emission spectra of 'Rockstar'-emitters on 6HX-nanotubes, taken at 225K. The green and blue lines are Gaussian fits of the emission from Tubes 4 and 5, with FWHM's of 59nm and 56nm respectively, around a 658nm peak.*

Figure 4.16 shows emission spectra of 'Rockstar'-emitters on 6HX-nanotubes at 225K. Gaussian fits show that FWHM's have narrowed to 59nm and 56nm for Tubes 4 and 5, respectively. Both are centered around 658nm emission. The intensity of the emission gathered from a spot on the tubes is generally lower than what is observed when the spectroscopy is performed at room temperature, though the variation in the intensity is quite large, as seen in the difference between Tubes 4 and 5.

4.3.2 Intensity

In order to observe the relative emission intensities of the 'Rockstar'-emitters on the 6HX-nanotubes compared to the emission from individual emitters, the intensity of the emitters on tubes in solution was measured while heating them up, using the same procedure as the one used for the DX-nanotubes (section 3.2.2).

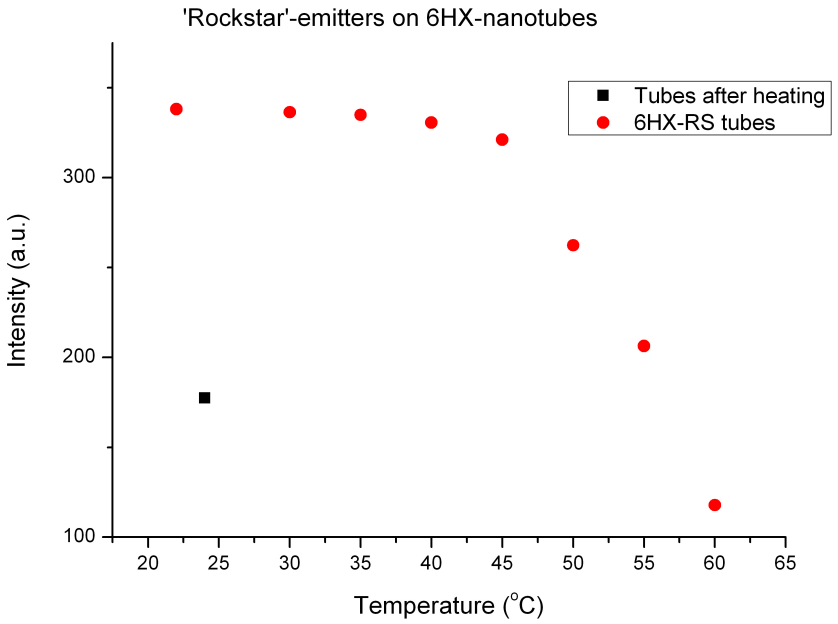

Figure 4.17: *Emission intensity of the 'Rockstar'-6HX-nanotube sample measured while the temperature of the solution is raised, measured by fluorimeter. Shown is the average intensity around the emission peak for 600nm excitation (red dots). The black square is the intensity after the sample was allowed to cool down to room temperature.*

The measured intensity of the 'Rockstar'-emitters on 6HX-nanotubes when the temperature is raised is shown in Figure 4.17. The emission of the sample decays when the temperature is increased above 45^{o}C, to a factor 3 decrease at 60^{o}C. After the sample is allowed to cool down, only a part of the emission is regained.

4.3.3 Intensity time-traces

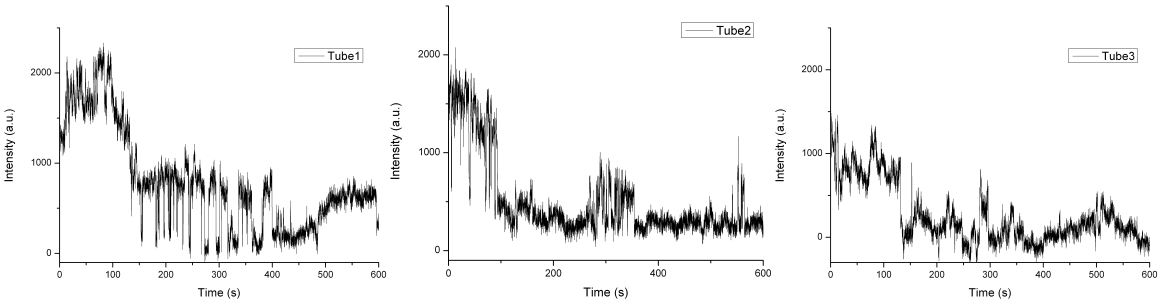

Figure 4.18: *Intensity time-traces of the emission from the emitters on 6HX-tubes shown in Figure 4.15. The measurements were done at room temperature. Blinking behavior manifests itself in the form of sharp steps in the emission intensity. The overall decay of the emission intensity over time is due to photobleaching of the individual emitters in the ensemble.*

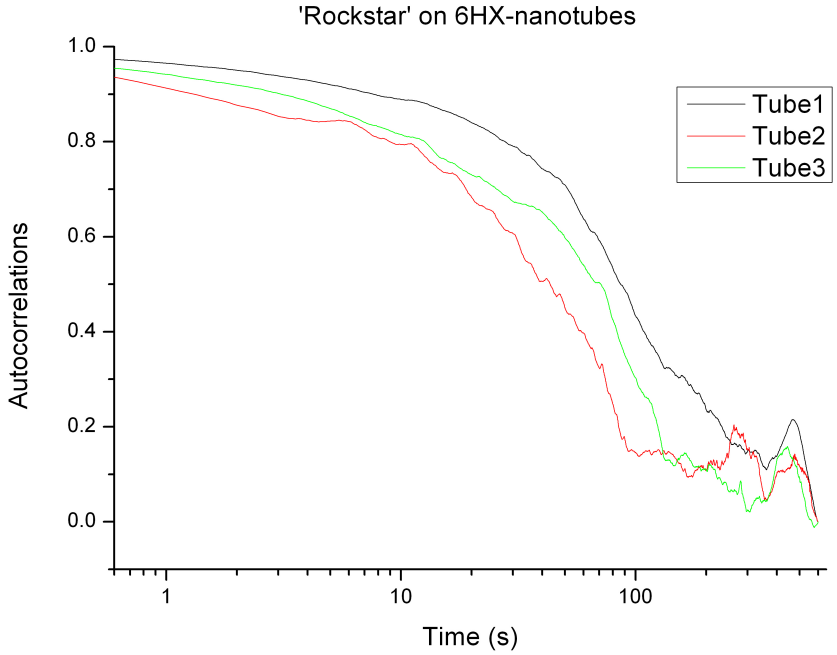

Figure 4.19: *Autocorrelation functions of the measured intensity shown in Figure 4.17. The autocorrelation function of the intensity-behavior of the emission from all three tubes with time show a peak around 460 seconds. The other noticeable peak is in the red line (Tube 2) and is around 260 seconds.*

Figure 4.18 and 4.19 show the results of intensity measurements taken over time of the emission from the emitters on 6HX-nanotubes corresponding to the emission spectra shown in Figure 4.15. The autocorrelation functions of the data show a significant peak for a shift of about 460 seconds, for all three individual tubes. The secondary peak around 260 seconds in the autocorrelation function for Tube 2 seems to correspond to the three separate 'packets' of blinking behavior that are visible in the raw intensity signal (Figure 4.18) around 20 seconds, around 300 seconds and around 550 seconds.

4.3.4 Discussion

Intensity

Unlike the hairpin-based emitters on the DX-nanotubes, the 'Rockstar' emitters on 6HX-nanotubes do not show an increased emission intensity when the temperature is raised.

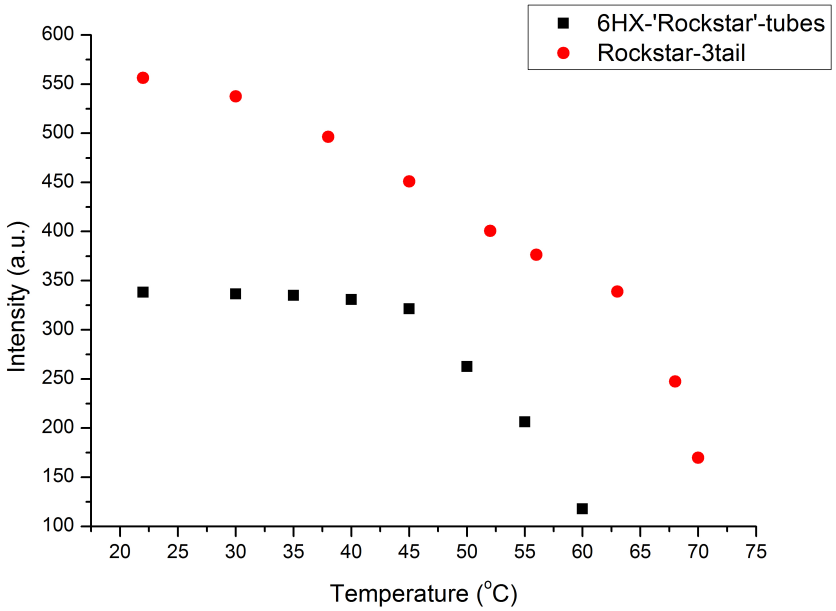

Figure 4.20: *Average intensity of the emission of a sample containing 'Rockstar'-emitters on 6HX-nanotubes vs single 'Rockstar'-emitters when the temperature is raised. The sample was excited with 600nm light. Both measurements show a decay in the emission when the temperature is raised.*

The 'Rockstar'-emitters show a similar decrease in intensity when they are on tubes as when they are separate (Figure 4.20). The decrease in intensity starts at a relatively high temperature for the emitters on tubes, indicating an increased melting temperature of the individual emitters due to an increased rigidity of the encapsulation when the strands are attached to the DNA-tube. Alternatively, it may point to a slight decrease in emission from the emitters on tubes by about 20%.

'Rockstar'-emitters have similar optical properties to hairpin-based emitters, but they show completely different behavior when compared to hairpin-based emitters when the temperature is raised. Because of this, emitter-emitter quenching is a less likely cause for the decreased emission from the hairpin-based emitters on DX-nanotubes.

The main difference, however, between the 'Rockstar'-strand and the pre-formed hairpins are the properties of the encapsulation. Because the 'Rockstar'-strand does not have a double-stranded part, the way the encapsulation around the silver cluster is formed can be different. This would mean that any 'pulling' or 'pushing' effect from the tubes, as was seen as a possible explanation for the intensity of the hairpins on DX-nanotubes, does not have the same effect of moving the cluster out of its optimal position, meaning the intensity of the emission is not disturbed by the presence of the tube.

Intensity time-traces

On average, a decrease of 4 steps can be seen in the emission intensity of the emitters on 6HX-nanotubes over the course of the measurements, indicating the bleaching of 4 individual emitters.

The individual tiles on the tube will be around 7 nm in length, meaning that there will be between 150 and 200 tiles in the beam spot, depending on the focus. As a result, the chemical yield

of fluorescent emitters forming on the 6HX-nanotube can be estimated to be around 3% after 3.5 hours. It is not unreasonable to think that more emitters would become measurably fluorescent if the sample had been given more time after the reduction. Given the increase in intensity of the emission from the sample in the next ∼10 hours after these measurements (by a factor around 2), the overall chemical yield of the forming of fluorescent emitters should be between 3-6%. Because these measurements were made in air and at room temperature, it can be expected that the emitters will be 'off' for a large portion of the time [5]. Because of this, there should be more than 4 emitters contributing to the emission, meaning the estimated chemical yield is most likely to be too low.

Measurements on three different tubes all show the same peak in the autocorrelation function after 460 seconds. This shows that there may be a level of ensemble-wide consistency in the state of the emission at this timescale.

Spectral properties

The spectra of the 'Rockstar'-emitters on 6HX-nanotubes (Figure 4.15) show around 70nm wide symmetrical Gaussian peaks. Considering the small number of emitters contributing, this can be considered unusual, because the individual emitters show emission peaks varying between 640nm and 675nm. The spectral diversity of the individual emitters makes it unlikely for a large number of very similar emitters to be contributing to a single emission spectrum. As a result, it's unlikely for the tube-spectra to be demonstrating such largely different, but symmetric spectra (646nm vs 674nm for the two fits in Figure 4.14). This leads us to believe that in both cases, a certain type of emitter is much more dominant in the emission than any others.

This could mean that part of the emitters that are present in the beam spot are not contributing to the emission, or that part of the emitters have not formed properly. This assessment is made more reasonable by the relatively low estimate for the chemical yield of the emitters forming on this tube (3-6%), compared to earlier estimates for the DX-nanotube structure [4] (45%).

If the chemical yield is indeed as low as the estimated 3-6% and if there are only 4-8 emitters in a beam spot, we are led to believe that the presence of a certain emitter might have an influence on the emission spectrum of other emitters on the tube, causing the emitters in the ensemble to emit on a similar wavelength. The frequency of an oscillation can be changed through introduction of another coupled oscillation within a certain frequency range [13], through injection locking. The locking range in the frequency domain is determined by, among other things, the relative amplitude of the injected signal as compared to that of the original oscillation. If the influence is more minor due to weaker coupling, the frequency will be 'pulled', without being completely locked to frequency of the injected signal.

Because the effect of the injection is dependent on the relative amplitudes of the two oscillations, varying numbers of individual spectrally different emitters may be able to have different effects on each others emission frequencies, causing the final collective emission to have a varying average frequency.

The resulting spectrum would be similar to a collection of individual emitters emittion within a small wavelength range, similar to what is seen in Figure 4.14.

Injection pulling between the emitters would induce a degree of coherence in the phase of the emission from the individual emitters on the tubes as well. Whilst the time-traces taken off these emitters are obviously, because they have a 100ms data interval, on a different timescale to the fluorescence of the emitters, if this phase-dependency at the shortest timescale results in a more well-defined phase of the system on the longer scale, this could explain the large peak(s) in the autocorrelation function of the time-traces in Section 4.3.3.

4.4 FRET-activity on 6HX-nanotubes

4.4.1 Measurements

The Cy3-dye molecules have emission spectra when attached to the 6HX-nanotubes which overlap with the absorption spectra of the 'Rockstar'-emitters on the tubes.

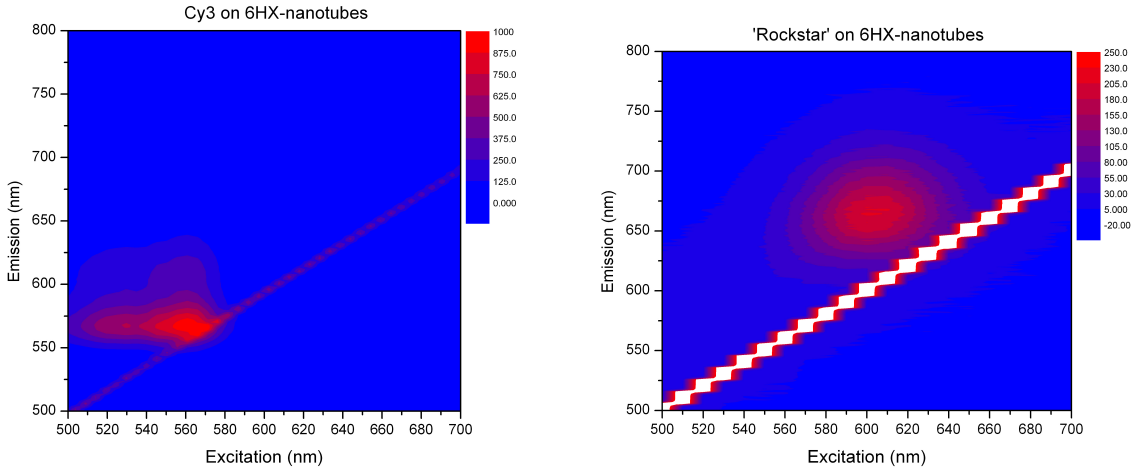

Figure 4.21: *Fluorimetries of Cy3 and 'Rockstar' on 6HX-nanotubes. Cy3 has a large emission peak around 565nm for a broad excitation range, and a secondary peak around 605nm for excitations above 540nm. This secondary peak is around the excitation for peak 'Rockstar'-emission (600nm). The units of intensity are not the same in both cases, the Cy3 has a much higher chemical and quantum yield.*

Figure 4.20 shows that the Cy3 can be used as a donor in FRET, if the 'Rockstar' on 6HX-nanotubes is functioning as an acceptor. The expectation would be that FRET activity would be maximized when the secondary emission-peak (around 605nm) of the Cy3 is maximally present, corresponding to excitations from 540-560nm.

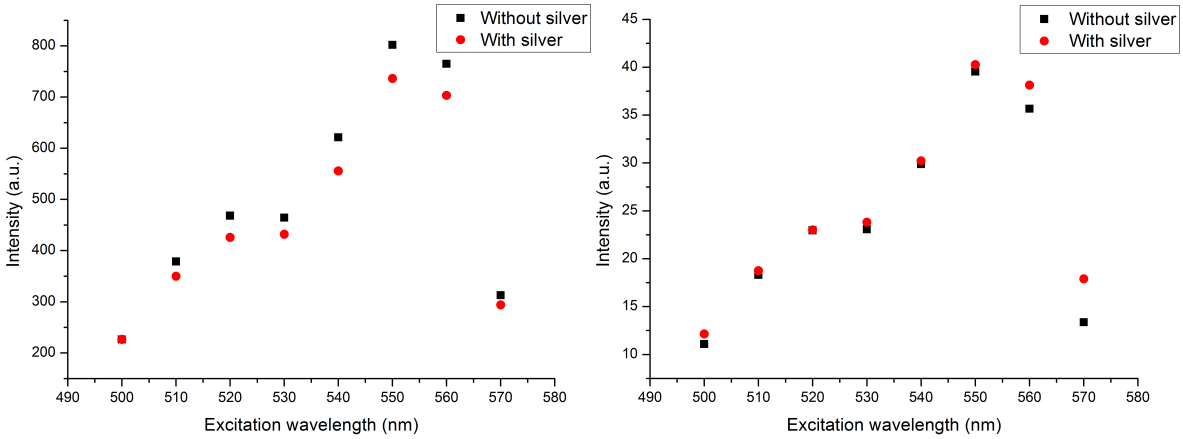

Figure 4.22: *Average intensity of the Cy3-emission (left) and of the 'Rockstar'-emission (right) of 6HX-nanotubes with both 'Rockstar'- and Cy3-modifications. The red dots and black squares constitute measurements on two batches of tubes, with and without adding silver and the reducing agent.*

Figure 4.21 shows the FRET-activity between Cy3 and 'Rockstar' on 6HX-nanotubes. A single batch of 6HX-nanotubes with modified U1-strands (Cy3) and modified U3-strands ('Rockstar') was split in two. Next, silver and reducing agent was added to one of the two using the established procedure for synthesizing the 'Rockstar'-emitters, and water was added to the other to keep the concentrations equal.

4.4.2 Discussion

The Cy3 shows a 10% decrease in emission when silver is added to the modified 6HX-nanotubes. Estimations of the chemical yield performed in section 4.3.4 led to a chemical yield of the forming of the 'Rockstar'-emitters of 3-6%.

Given the amount of FRET-activity, the 3-6% estimate for the chemical yield of the formation of fluorescent silver clusters was probably too low. It also means that the FRET-efficiency is expected to be very high. As a result, it would seem that the emitters are positioned as intended on the 6HX-nanotubes. The 5'-ends of the U1- and U3-strands have at least one full 3nm-wide tile between them, making the distance between the Cy3 and the place where the 'Rockstar' is connected to the tube expected to be around 4nm. Such a high FRET-efficiency, despite what is probably not a perfect spectral overlap (thus, a relatively short Förster radius), also leads us to believe that the silver cluster itself is close to the tube structure, and is likely to be close (within 3nm) to the 3'-end of the 'Rockstar'-strand in its final position.

There is a difference between the measurements performed on tubes with or without silver clusters due to presence of stray silver in the sample. However, considering the decreased intensity of Cy3 is limited to the excitation wavelengths where FRET-activity would be expected it seems reasonable to attribute a significant part of this decrease to transfer of energy to the 'Rockstar'-emitters through FRET.

The emission of the sample around 660nm becomes slightly brighter, due to a small amount of emission from 'Rockstar'-emitters when compared to the Cy3-emission. The exact increase in the 'Rockstar'-emission is hard to determine due to relatively large contributions from the Cy3 in this wavelength range, and the small chemical yield of the 'Rockstar'-emitter synthesis.

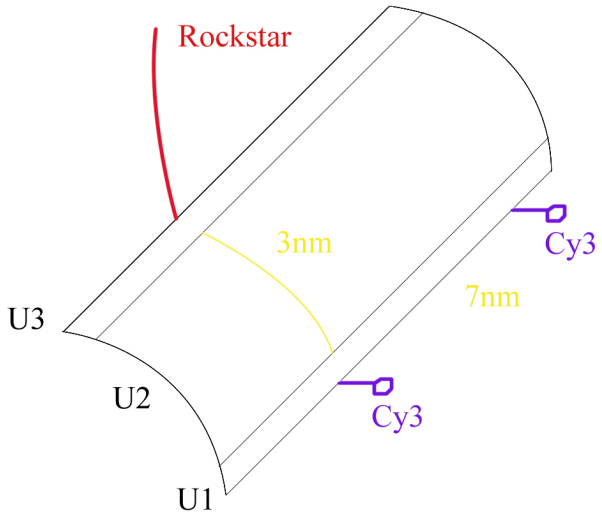

Figure 4.23: *Representation of a part on the 6HX-tube structure. The width of the U2-strand is 3nm. It is unknown how much of the U3- and U1-strands will be between the Cy3 and 'Rockstar', making a 4nm distance a conservative estimate. The Cy3 can be expected to be on all the U1-strands, the 'Rockstar'-emitters are expected to occupy no more than 10% of the U3-strands.*

Chapter 5

Conclusion

In order to observe the behavior of DNA-encapsulated silver clusters when they are placed in close proximity on larger DNA-nanostructures, they have been placed on two different type of DNA-nanotube. A comparison has been made with regard to the spectral properties and emission intensity between individual fluorescent silver clusters and those placed on these nanotube structures. 6HX-nanotubes allow the emitters to be placed on pre-programmed sites along the circumference, allowing much more well-defined placement of different or similar emitters in the future. Observing directional effects may also become a possibility using these tubes.

Observations have been made on the optical behavior of fluorescent silver clusters when they are placed on these DNA-nanotubes, in order to gain an insight into the behavior of these emitters when they are placed on large DNA-nanostructures.

It has been shown that the emission intensity of an ensemble of hairpin-based emitters is diminished when they are placed on the nanotube structure. When the tubes are heated and broken, an increased intensity indicates a change in the quantum yield of the emitters when they are in close proximity on a DNA-nanotube. Alternatively, conformational changes to the silver clusters or to their encapsulations can cause an increase in the overall amount of visibly fluorescent silver clusters when they are heated and become separated from the tubes.

Because this effect is not present for the 'Rockstar'-emitters, which emit at a similar wavelength, but have a different encapsulation, a positional or conformational change to the silver cluster seems to be the most likely cause. Because the tile-structure containing the hairpins should be broken at a higher temperature, changes to the encapsulation should be minor, leading us to believe that the properties of the silver cluster itself may be altered by the presence of the DNA-tube. In order to investigate this behavior further, accurate absorption measurements on the emitters on DX-nanotubes in different conditions can show whether the decreased emission is the result of decreased quantum yield, or of a lower effective chemical yield through changes in the properties of the individual silver clusters in their encapsulations.

For individual emitters, a longer stem has been shown to induce an increased intensity for higher temperatures as well, which can be attributed to a gradual loosening of the encapsulation when some of the base-pairs become separated.

Spectroscopy and measurements on the intensity behavior with time have been made in order to find possible interactions between individual emitters on the DNA-tube. It has been shown that for a large collection of hairpin-based emitters on a DX-nanotube, the emitters behave as a large ensemble of individual emitters. As a result, we conclude that there are probably no ensemble-wide interactions for hundreds of emitters in close proximity on a DX-nanotube.

When a smaller ensemble of emitters is placed on a 6HX-nanotube at spacings in the order of 100nm, spectral measurements show somewhat surprisingly symmetrical and narrow emission spectra. The emitters do not seem to behave as several individually picked emitters in this case.

Intensity time-traces of this ensemble shows a correlation between the initial state of the system and the system at a relatively long timescale of 460 seconds. These indicate a level of coherence between the state of the individual emitters, and may point towards interesting interactions between them. Because the emitters fall within a set frequency range, phase-locking between the individual emitters can cause the emitters to be pulled towards eachother in the frequency domain, whilst inducing a more well-defined phase in the system at the shortest timescale. Performing spectroscopy measurements on these emitter-ensembles at very low temperatures can shed additional light on this behavior by narrowing the emission spectra from the individual emitters further.

It is very likely that FRET-activity has been observed through placement of the 'Rockstar'-Ag:DNA's in close proximity to Cy3-fluorophores on the 6HX-nanotube structure. The decrease in intensity of the donor indicates a strong FRET-efficiency, though the low chemical yield of the 'Rockstar'-emitters makes accurate FRET-measurements a challenge. Using Ag:DNA's as donors in these experiments would allow increased visibility of acceptor-emission through a lower background of emission from the donor.

Bibliography

[1] J.T. Petty, J. Zheng, N.V. Hud, and R.M. Dickson. DNA-templated Ag nanocluster formation. *Journal of the American Chemical Society*, 126(16):5207–5212, APR 28 2004.

[2] E. Gwinn, P.R. O'Neill, A. J. Guerrero, D. Bouwmeester, and D.K. Fygenson. Sequence-dependent fluorescence of DNA-hosted silver nanoclusters. *Advanced Materials*, 20(2):279+, JAN 18 2008.

[3] P.W.K. Rothemund. Folding DNA to create nanoscale shapes and patterns. *Nature*, 440(7082):297–302, MAR 16 2006.

[4] P.R. O'Neill, K. Young, D. Schiffels, and D.K. Fygenson. Few-Atom Fluorescent Silver Clusters Assemble at Programmed Sites on DNA Nanotubes. *Nano Letters*, 12(11):5464–5469, NOV 2012.

[5] S.S.R. Oemrawsingh, N. Markesevic, E.G. Gwinn, E.R. Eliel, and D. Bouwmeester. Spectral Properties of Individual DNA-Hosted Silver Nanoclusters at Low Temperatures. *Journal of Physical Chemistry C*, 116(48):25568–25575, DEC 6 2012.

[6] P.R. O'Neill, L.R. Velazquez, D.G. Dunn, E.G. Gwinn, and D.K. Fygenson. Hairpins with Poly-C Loops Stabilize Four Types of Fluorescent Ag-n:DNA. *Journal of Physical Chemistry C*, 113(11):4229–4233, MAR 19 2009.

[7] K. Fujibayashi, R. Hariadi, S.H. Park, E. Winfree, and S. Murata. Toward reliable algorithmic self-assembly of DNA tiles: A fixed-width cellular automaton pattern. *Nano Letters*, 8(7):1791–1797, JUL 2008.

[8] P. Yin, R.F. Hariadi, S. Sahu, H.M.T. Choi, S.H. Park, T.H. LaBean, and J.H. Reif. Programming DNA tube circumferences. *Science*, 321(5890):824–826, AUG 8 2008.

[9] R. Clegg. *FRET and FLIM Techniques. Laboratory Techniques in Biochemistry and Molecular Biology.* Elsevier, 2009.

[10] R. Adler. Study of Locking Phenomena in Ocillator. *Proceedings of the IEEE*, 61(10):1380–1385, 1973.

[11] P. Bhansali and J. Roychowdhury. Gen-adler: The generalized adler's equation for injection locking analysis in oscillators. pages 522–527, 2009.

[12] H.L. Stover and W.H. Steier. Locking of Laser Oscillators by Light Injection. *Applied Physics Letters*, 8(4):91–&, 1966.

[13] C.L. Tang and H. Statz. Phase-Locking of Laser Oscillators by injected signal. *Journal of Applied Physics*, 38(1):323–&, 1967.

Appendix A

Strand sequences

A.1 Single emitters

'Rockstar' CAC CGC TTT TGC CTT TTG GGG ACG GAT A

9C-'jstem' TAC-TTA-CCT-CCC-CCC-CCC-AGG-TAA-GTA-TT

A.2 DX-nanotubes

SE1 CTC-AGT-GGA-CAG-CCG-TTC-TGG-AGC-GTT-GGA-CGA- AAC-T

SE1-9C CTC-AGT-GGA-CAG-CCT-ACT-TAC-CT-CCC-CCC-CCC-A-GGT-AAG-TAT-TGT-TCT-GGA-GCG-TTG-GAC-GAA-ACT

SE1-7C CTC-AGT-GGA-CAG-CCT-ACT-TAC-CT-CCC-CCC-C-A- GGT-AAG-TAT-TGT-TCT-GGA-GCG-TTG-GAC-GAA-ACT

SE1-6CA2 CTC-AGT-GGA-CAG-CCT-ACT-TAC-CT-CAC-CCC-A-GGT- AAG-TAT-TGT-TCT-GGA-GCG-TTG-GAC-GAA-ACT

SE2 GTC-TGG-TAG-AGC-ACC-ACT-GAG-AGG-TA

SE3 CCA-GAA-CGG-CTG-TGG-CTA-AAC-AGT-AAC-CGA-AGC- ACC-AAC-GCT

SE3-FAM CCA-GAA-CGG-CTG-TGG-CTA-AAC-AGT-AAC-CGA-AGC- ACC-AAC-GCT/36-FAM

SE4 CAG-ACA-GTT-TCG-TGG-TCA-TCG-TAC-CT

SE5 CGA-TGA-CCT-GCT-TCG-GTT-ACT-GTT-TAG-CCT-GCT- CTA-C

A.3 HX-nanotubes

U1 GGCGATTAGG-ACGCTAAGCCA-CCTTTAGATCC-TGTATCTGGT

U1-Cy3 /5Cy3/TT-GGCGATTAGG-ACGCTAAGCCA-CCTTTAGATCC-TGTATCTGGT

U2 GGATCTAAAGG-ACCAGATACA-CCACTCTTCC-TGACATCTTGT

U3 GGAAGAGTGG-ACAAGATGTCA-CCGTGAGAACC-TGCAATGCGT

U4 GGTTCTCACGG-ACGCATTGCA-CCGCACGACC-TGTTCGACAGT

U5 GGTCGTGCGG-ACTGTCGAACA-CCAACGATGCC-TGATAGAAGT

T6 GGCATCGTTGG-ACTTCTATCA-CCTAATCGCC-TGGCTTAGCGT

Appendix B

Recipes

B.1 Single emitters

B.1.1 7C-hairpins

Final concentrations:

7C-hairpins 15μM

NH_4OAc 6.75mM

AgNO3 160μM

$NaBH_4$ 25μM

$AgNO_3$ was added to the DNA in the NH_4OAc buffer, after which the sample was kept refrigerated ($\sim 4^oC$) for 30 mins before addition of $NaBH_4$.

B.1.2 9C-hairpins/9C-'jstem' hairpins/9C-3tail hairpins

Final concentrations:

9C-hairpins 50μM

NH_4OAc 20mM

AgNO3 350μM

$NaBH_4$ 100μM

$AgNO_3$ was added to the DNA in the NH_4OAc buffer, after which the sample was kept refrigerated ($\sim 4^oC$) for 30 mins before addition of $NaBH_4$.

B.1.3 'Rockstar'

Final concentrations:

'Rockstar'-strands 15μM

NH_4OAc 6.75mM

AgNO3 145μM

$NaBH_4$ 72.5μM

$AgNO_3$ was added to the DNA in the NH_4OAc buffer, after which the sample was kept refrigerated ($\sim 4^oC$) for 40 mins before addition of $NaBH_4$.

B.2 DX-nanotubes

Final concentrations:

SE1-9C/7C 2μM

SE2 2μM

SE3/SE3-FAM 2μM

SE4 2μM

SE5 2μM

NH_4OAc 40mM

MgOAc 10mM

FAM is used as a fluorescent marker if necessary to confirm the tube-annealing process.

B.3 6HX-nanotubes

Final concentrations:

U1 3μM

U2 3μM

U3 3μM

U4 3μM

U5 3μM

T6 3μM

NH_4OAc 20mM

MgOAc 12.5mM

Appendix C

Equipment

C.1 Single Molecule-Spectroscopy Setup

Filters:

579/34nm BrightLine Bandpass Filter, Semrock 01-579/34-25

593nm BrightLine LWP Edge Filter, Semrock 01-593/LP-25

647/57nm BrightLine Bandpass Filter, Semrock 01-647/57-25

600nm Longpass filter, Thorlabs FEL0600

605nm Dichroic Beamsplitter, 25.2 x 35.6 mm, Semrock 605-Di02-25x36

Other equipment:

CCD-Camera Andor Technology, iKon CCD-08061

Dye Laser Coherent899 Ring Laser Quantum Running on Rhodamine 6G dye

Spectrometer Ocean Optics QE 65000

Cryostat Leiden FMD

Noise eater 2343-23 06 Noise eater (Crystal) Gsanger LM 0202 AR 632nm

Photon counter Perkin Elmer SPCM-AQR-14-FC

Fast steering mirror Newport FSM-300 Series

Time tagging card Cronologic HPTDC 8-PC1

Mirrors pinholes, lenses etc. ThorLabs

For basic alignment a He:Ne laser was used, combined with a small CCD-camera.